Noname manuscript No. (will be inserted by the editor)

Second-order decoupled linear energy-law preserving gPAV numerical schemes for two-phase flows in superposed free flow and porous media

Yali Gao and Daozhi Han

the date of receipt and acceptance should be inserted later

Abstract We propose second-order numerical methods based on the generalized positive auxiliary variable (gPAV) framework for solving the Cahn-Hilliard-Navier-Stokes-Darcy model in superposed free flow and porous media. In the gPAV-reformulated system, we introduce an auxiliary variable according to the modified energy law and take account into the interface conditions between the two subdomains. By implicit-explicit temporal discretization, we develop fully decoupled linear gPAV-CNLF and gPAV-BDF2 numerical methods effected with the Galerkin finite element method. The fully discrete schemes satisfy a modified energy law irrespective of time step size. Plentiful numerical experiments are performed to validate the methods and demonstrate the robustness. The application in filtration systems, the influence of viscous instability, general permeability, curve interface, and different densities are discussed in details to further illustrate the compatibility and applicability of our developed gPAV numerical methods.

 $\textbf{Keywords} \ \ \text{Cahn-Hilliard-Navier-Stokes-Darcy} \ \ \text{model} \cdot \ \text{gPAV} \ \ \text{approach} \cdot \ \text{unconditionally} \ \ \text{stability} \cdot \ \ \text{artificial compression} \cdot \ \text{second order} \ \ \text{accuracy}$

Mathematics Subject Classification (2010) 65M15 · 65M12 · 65M60 · 76D05

1 Introduction

The Cahn-Hilliard-Navier-Stokes-Darcy (CHNSD) model [32, 34] is an important diffuse interface model that describes two-phase flow in superposed free flow and porous media. It has many applications, including water management in proton exchange membrane (PEM) fuel cells [22, 60], industrial filtration, fluid displacement in oil reservoirs [9], groundwater contamination in karst aquifers, and droplet formation in microfluidic technology [2, 72]. On the other hand, the CHNSD system is a typical multiphysics, multi-domain problem that comprises the Cahn-Hilliard-Navier-Stokes equations governing two-phase flow in free flow region, the Cahn-Hilliard-Darcy system for two-phase flow in porous media, and a set of domain interface boundary conditions [25, 34]. Han [34] established global existence of weak solutions and weak-strong uniqueness to the CHNSD system. One of distinct features of the model is its automatic capturing of topological transitions of the interface [44, 50], at the expense of the stiffness resulting from large spatial gradients across the thin interface layer [20].

In recent years many works have emerged for solving the CHNSD model [10, 12, 23, 25]. Chen [10] proposed partially and totally decoupled numerical methods for Cahn-Hilliard-Stokes-Darcy system by combining operator splitting, pressure stabilization and convex splitting methods, then rigorously analyzed its unique solvability and energy stability. Gao [25] constructed a decoupled numerical method to simulate CHNSD system taking account for two Cahn-Hilliard equations in free flow region and porous media region, respectively. Chen [11] considered the CHNSD model with thermal convection of two-phase flow, and proposed unconditionally stable numerical methods to independently solve Navier-Stokes equations, Darcy equations, heat equations, and the Cahn-Hilliard equations at each time level.

School of Mathematics and Statistics, Northwestern Polytechnical University, Xi'an Shaanxi, 710129, P.R.China E-mail: gaoylimath@nwpu.edu.cn

D. Han

Department of Mathematics, Department of Mathematics, The State University of New York at Buffalo, Buffalo, NY 14260 USA E-mail: daozhiha@buffalo.edu

Y. Gac

Even though efficient numerical methods of first order accuracy exist, to the best of our knowledge, this work contributes to the first second order accurate numerical schemes for the CHNSD model.

There are several techniques in the literature for dealing with the stiffness of phase field model, such as convex-splitting strategy [3, 28, 55], stabilization method [21, 57, 63], the Invariant Energy Quadratization (IEQ) approach [41, 62, 66, 51], scalar auxiliary variable (SAV) approach [53, 56, 64, 71], generalized positive auxiliary variable (gPAV) approach [46, 52, 68], and the zero-energy-contribution approach [65, 67, 69, 70]. The gPAV method has remarkable properties: resulting linear algebraic system with constant coefficient matrices, preserving positivity of the scalar variable, and simplifying treatment complex interface conditions and boundary conditions [45, 52]. Therefore, we shall build a gPAV framework taking into account interface conditions between free flow region and porous media to develop linear numerical schemes for the CHNSD system. Furthermore, decoupled numerical schemes allowing larger time step size are in great need to further improve the computational efficiency and make long-time simulations of more realistic problems feasible, especially for hydraulic conductivity tensor with small eigenvalues [38, 43]. The decoupling of fluid equations can be achieved by exploiting pressure projection [30, 58, 40, 48], artificial compressible method [18, 29, 37], artificial viscosity [42].

In this contribution we focus on the development of unconditionally stable, totally decoupled, second-order in time and linear numerical schemes based on the gPAV framework for the CHNSD model. By introducing an auxiliary scalar variable according to the modified discrete energy from the artificial compression method, we reformulate the CHNSD system into an equivalent system that incorporates interface conditions. We then exploit implicit-explicit discretization to deal with the coupling between two different sub-regions and the coupling between the phase field equation and the fluid equations. Stabilization via artificial viscosity is incorporated to further improve the accuracy and stability. Finite element method is adopted for spatial discretization. By using the Crank-Nicolson leap-frog time-marching (CNLF) and the second-order backward differentiation formula (BDF2), respectively, we design two numerical methods, termed as the gPAV-CNLF scheme and the gPAV-BDF2 scheme. We then rigorously establish the unconditional stability, in the sense of monotonically decreasing of the modified discrete energy, for both the gPAV-CNLF and the gPAV-BDF2 numerical schemes.

The rest of paper is organized as follows. In Section 2, we present the CHNSD model, derive the equivalent gPAV system and propose its weak formulation satisfying a modified energy law. In Section 3, fully decoupled numerical schemes of second order accuracy, i.e. gPAV-CNLF and gPAV-BDF2 algorithms, are constructed, the energy stability are then rigorously proved. In Section 4, we discuss the implementations issues for both gPAV-CNLF and gPAV-BDF2 methods. In Section 5, ample numerical experiments are carried out to illustrate the desirable features of proposed decoupled numerical methods.

2 Cahn-Hilliard-Navier-Stokes-Darcy model

In this section, we first give a brief introduction for the Cahn-Hilliard-Navier-Stokes-Darcy model, derive the equivalent system based on gPAV framework and its weak formulation, and show the dissipative energy law for the reformulated gPAV system.

2.1 Model system

Consider a bounded domain $\Omega = \Omega_c \bigcup \Omega_m \subset \mathbb{R}^d \, (d=2,3)$ consisting of free-flow region Ω_c and porous media region Ω_m . We assume the Lipschitz continuous boundaries $\partial \Omega_c$ and $\partial \Omega_m$, and form the interface $\Gamma = \partial \Omega_m \cap \partial \Omega_c$, $\Gamma_m = \partial \Omega_m \backslash \Gamma$, and $\Gamma_c = \partial \Omega_c \backslash \Gamma$. Let \mathbf{n}_c and \mathbf{n}_m be the unit outer normal to the fluid and the porous media regions at the interface Γ , respectively. A typical geometry is illustrated in Figure 1.

Consider homogeneous free energy $F(\phi)$ with a double-well polynomial $F(\phi) = \frac{1}{4\epsilon}(\phi^2 - 1)^2$, and let $f(\phi) = F'(\phi)$ associated with the capillary width ϵ of the thin interfacial region. Denote ϕ_j (j = c, m) be a phase function indicating two different fluids by taking distinct ± 1 . Variable w_j (j = c, m) represents the chemical potential depended on phase variable ϕ_j . Mobility M_j (j = c, m) is a diffusion coefficient and may related to phase function ϕ [14]. Parameter γ describes the elastic relaxation time.

Two-phase flow in porous media region Ω_m is assumed to satisfy the Cahn-Hilliard-Darcy (CHD) equations

$$\mathbb{K}^{-1}\boldsymbol{u}_m + \nabla p_m - w_m \nabla \phi_m = 0, \tag{2.1}$$

$$\nabla \cdot \boldsymbol{u}_m = g(\boldsymbol{x}), \tag{2.2}$$

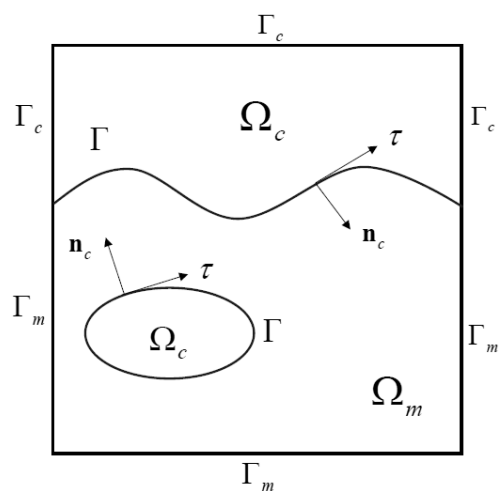


Fig. 1: A sketch of the porous media domain Ω_m , free fluid domain Ω_c , and the interface Γ .

$$\frac{\partial \phi_m}{\partial t} + \boldsymbol{u}_m \cdot \nabla \phi_m - \nabla \cdot (M_m(\phi_m) \nabla w_m) = h_m(\boldsymbol{x}), \tag{2.3}$$

$$w_m + \gamma \epsilon \triangle \phi_m - \frac{\gamma}{\epsilon} f(\phi_m) = 0, \qquad (2.4)$$

where u_m denotes the fluid discharge rate in the porous media, p_m denotes the hydraulic head, and \mathbb{K} denotes the hydraulic conductivity tensor that satisfies the relation $\mathbb{K} = \frac{\Pi}{\nu(\phi_m)}$. (2.3)-(2.4) take into account the diffusion of the order parameter ϕ and the interfacial energy between two phase, allowing for simulation of phase separation and interface dynamics.

Two-phase flow in the fluid region Ω_c is governed by the Cahn-Hilliard-Navier-Stokes (CHNS) equations

$$\frac{\partial \boldsymbol{u}_c}{\partial t} + (\boldsymbol{u}_c \cdot \nabla) \boldsymbol{u}_c - \nabla \cdot \mathbb{T}(\boldsymbol{u}_c, p_c) - w_c \nabla \phi_c = \boldsymbol{f}(\boldsymbol{x}), \tag{2.5}$$

$$\nabla \cdot \boldsymbol{u}_c = 0, \tag{2.6}$$

$$\frac{\partial \phi_c}{\partial t} + \boldsymbol{u}_c \cdot \nabla \phi_c - \nabla \cdot (M_c(\phi_c) \nabla w_c) = h_c(\boldsymbol{x}), \tag{2.7}$$

$$w_c + \gamma \epsilon \triangle \phi_c - \frac{\gamma}{\epsilon} f(\phi_c) = 0,$$
 (2.8)

where $\mathbb{T}(\boldsymbol{u}_c, p_c) = 2\nu(\phi_c)\mathbb{D}(u_c) - p_c\mathbb{I}$ is the stress tensor with deformation tensor $\mathbb{D}(u_c) = (\nabla \boldsymbol{u}_c + \nabla^T \boldsymbol{u}_c)/2$ and identity matrix \mathbb{I} . Variables \boldsymbol{u}_c and p_c are the fluid velocity and the kinematic pressure, and ν prescribes the kinematic viscosity of the fluid, $0 < c \le \nu$ with positive constant c.

The two systems are coupled though a set of domain interface boundary conditions along the interface Γ as follows [10, 24, 32].

$$\phi_m = \phi_c, \tag{2.9}$$

$$w_c = w_m, (2.10)$$

$$\nabla \phi_c \cdot \boldsymbol{n}_c = -\nabla \phi_m \cdot \boldsymbol{n}_m, \tag{2.11}$$

$$M_c(\phi_c)\nabla w_c \cdot \boldsymbol{n}_c = -M_m(\phi_m)\nabla w_m \cdot \boldsymbol{n}_m, \tag{2.12}$$

$$\boldsymbol{u}_c \cdot \boldsymbol{n}_c = -\boldsymbol{u}_m \cdot \boldsymbol{n}_m, \tag{2.13}$$

$$-\boldsymbol{n}_c \cdot (\mathbb{T}(\boldsymbol{u}_c, p_c) \cdot \boldsymbol{n}_c) = p_m - \frac{1}{2} |\boldsymbol{u}_c|^2, \tag{2.14}$$

$$-\boldsymbol{\tau}_{j} \cdot (\mathbb{T}(\boldsymbol{u}_{c}, p_{c}) \cdot \boldsymbol{n}_{c}) = \frac{\alpha \nu \sqrt{d}}{\sqrt{\operatorname{trace}(\boldsymbol{\Pi})}} \boldsymbol{\tau}_{j} \cdot \boldsymbol{u}_{c}, \tag{2.15}$$

where τ_j $(j=1,\cdots,d-1)$ stands for mutually orthogonal unit tangential vectors, and Π is the permeability of the porous media. (2.9)-(2.12) accounts for the continuity conditions for the phase field function, the chemical potential, and their normal derivatives [32, 35]. (2.13) represents the continuous of velocity, (2.14) describes the balance of the forces with the inertial forces [32, 6, 27], and (2.14) is the well-known Beavers-Joseph-Saffman-Jones (BJS) interface condition [4].

For simplicity, we consider the following boundary conditions

$$p_m|_{\Gamma_m} = 0, \ \nabla \phi_m \cdot \boldsymbol{n}_m|_{\Gamma_m} = 0, \ M_m(\phi_m) \nabla w_m \cdot \boldsymbol{n}_m|_{\Gamma_m} = 0, \tag{2.16}$$

$$\mathbf{u}_c|_{\Gamma_c} = 0, \ \nabla \phi_c \cdot \mathbf{n}_c|_{\Gamma_c} = 0, \ M_c(\phi_c) \nabla w_c \cdot \mathbf{n}_c|_{\Gamma_c} = 0,$$
 (2.17)

and initial conditions

$$\phi_c(0, \mathbf{x}) = \phi_c^0(\mathbf{x}), \ \phi_m(0, \mathbf{x}) = \phi_m^0(\mathbf{x}), \ \mathbf{u}_c(0, \mathbf{x}) = \mathbf{u}_c^0(\mathbf{x}).$$
 (2.18)

Without loss of generality, we also assume that \mathbb{K} is a bounded, symmetric and uniformly positive definite matrix.

The total energy associated with the CHNSD system is [25]

$$\widetilde{E}(\boldsymbol{u}_c, \phi) = \int_{\Omega_c} \frac{1}{2} |\boldsymbol{u}_c|^2 d\boldsymbol{x} + \gamma \int_{\Omega} \left(\frac{\epsilon}{2} |\nabla \phi|^2 + \frac{1}{\epsilon} F(\phi) \right) d\boldsymbol{x}.$$
(2.19)

2.2 Reformulated equivalent system

To facilitate the design of decoupled second-order numerical algorithms for the system (2.1)-(2.4), (2.5)-(2.8) and (2.9)-(2.17), we reformulate it according to the gPAV framework. In general, we use the standard Sobolev spaces, introduce $H^m(\Omega) = W^{m,2}(\Omega)$ with the norm $\|\cdot\|_m$. Denote the essential supremumm by $\|\cdot\|_{\infty}$, L^2 norm by $\|\cdot\|$.

We first exploit the artificial compressibility method and replace the divergence-free condition by [18, 29]

$$2\epsilon_2 \frac{\partial p_c}{\partial t} + \nabla \cdot \boldsymbol{u}_c = 0,$$

where ε_2 is a constant to be determined later. Introducing the modified energy

$$E(\boldsymbol{u}_c, \phi) = \int_{\Omega_c} \frac{1}{2} |\boldsymbol{u}_c|^2 d\boldsymbol{x} + \gamma \int_{\Omega} \left(\frac{\epsilon}{2} |\nabla \phi|^2 + \frac{1}{\epsilon} F(\phi) \right) d\boldsymbol{x} + \varepsilon_2 \int_{\Omega_c} |p_c|^2 d\boldsymbol{x},$$
 (2.20)

we introduce two scalar auxiliary variables such that

$$R(t) = \sqrt{E(\boldsymbol{u}_c, \phi)}, \quad \xi = \frac{R^2}{E},$$

then, taking the time derivative and using (2.20), R(t) satisfies following evolution equation

$$2R\frac{dR}{dt} = (\frac{\partial \boldsymbol{u}_c}{\partial t}, \boldsymbol{u}_c) + \gamma \epsilon (\nabla \phi, \nabla \frac{\partial \phi}{\partial t}) + 2\epsilon_2 (\frac{\partial p_c}{\partial t}, p_c) + \xi \frac{\gamma}{\epsilon} (f(\phi), \frac{\partial \phi}{\partial t}). \tag{2.21}$$

Following the idea of gPAV, we incorporate the zero terms into the right hand side of (2.21) to obtain

$$2R\frac{dR}{dt} = (\frac{\partial \boldsymbol{u}_{c}}{\partial t}, \boldsymbol{u}_{c}) + \gamma \epsilon(\nabla \phi, \nabla \frac{\partial \phi}{\partial t}) + 2\epsilon_{2}(\frac{\partial p_{c}}{\partial t}, p_{c}) + \xi \frac{\gamma}{\epsilon}(f(\phi), \frac{\partial \phi}{\partial t})$$

$$- \left[-2\nu(\mathbb{D}(\boldsymbol{u}_{c}), \mathbb{D}(\boldsymbol{u}_{c})) + (p_{c}, \nabla \cdot \boldsymbol{u}_{c}) - \xi((\boldsymbol{u}_{c} \cdot \nabla)\boldsymbol{u}_{c}, \boldsymbol{u}_{c}) + \xi(\boldsymbol{w}_{c}\nabla\phi_{c}, \boldsymbol{u}_{c}) - \frac{\xi}{2}((\nabla \cdot \boldsymbol{u}_{c})\boldsymbol{u}_{c}, \boldsymbol{u}_{c}) \right]$$

$$- (\nabla \cdot \boldsymbol{u}_{c}, p_{c}) - (\mathbb{K}^{-1}\boldsymbol{u}_{m}, \boldsymbol{u}_{m}) - (\nabla p_{m}, \boldsymbol{u}_{m}) + \xi(\boldsymbol{w}_{m}\nabla\phi_{m}, \boldsymbol{u}_{m}) + (\boldsymbol{u}_{m}, \nabla p_{m}) - M(\nabla \boldsymbol{w}, \nabla \boldsymbol{w})$$

$$- \xi(\boldsymbol{u} \cdot \nabla \phi, \boldsymbol{w}) + (\boldsymbol{f}(\boldsymbol{x}), \boldsymbol{u}_{c}) + (g(\boldsymbol{x}), p_{m}) + (h(\boldsymbol{x}), \boldsymbol{w})] + \frac{\alpha\nu\sqrt{d}}{\sqrt{\text{trace}(\boldsymbol{\Pi})}} \langle P_{\tau}\boldsymbol{u}_{c}, P_{\tau}\boldsymbol{u}_{c} \rangle$$

$$+ \xi \langle p_{m} - \frac{1}{2}|\boldsymbol{u}_{c}|^{2}, \boldsymbol{u}_{c} \cdot \boldsymbol{n}_{c} \rangle - \xi \langle \boldsymbol{u}_{c} \cdot \boldsymbol{n}_{c}, p_{m} \rangle$$

$$+ \xi \left[-2\nu(\mathbb{D}(\boldsymbol{u}_{c}), \mathbb{D}(\boldsymbol{u}_{c})) + (p_{c}, \nabla \cdot \boldsymbol{u}_{c}) - ((\boldsymbol{u}_{c} \cdot \nabla)\boldsymbol{u}_{c}, \boldsymbol{u}_{c}) + (\boldsymbol{w}_{c}\nabla\phi_{c}, \boldsymbol{u}_{c}) - \frac{1}{2}((\nabla \cdot \boldsymbol{u}_{c})\boldsymbol{u}_{c}, \boldsymbol{u}_{c}) \right]$$

$$- (\nabla \cdot \boldsymbol{u}_{c}, p_{c}) - (\mathbb{K}^{-1}\boldsymbol{u}_{m}, \boldsymbol{u}_{m}) - (\nabla p_{m}, \boldsymbol{u}_{m}) + (\nabla p_{m}, \boldsymbol{u}_{m}) + (\boldsymbol{w}_{m}\nabla\phi_{m}, \boldsymbol{u}_{m}) - (M\nabla \boldsymbol{w}, \nabla \boldsymbol{w})$$

$$- (\boldsymbol{u} \cdot \nabla \phi, \boldsymbol{w}) - \langle p_{m} - \frac{1}{2}|\boldsymbol{u}_{c}|^{2}, \boldsymbol{u}_{c} \cdot \boldsymbol{n}_{c} \rangle + \langle \boldsymbol{u}_{c} \cdot \boldsymbol{n}_{c}, p_{m} \rangle + \frac{\alpha\nu\sqrt{d}}{\sqrt{\text{trace}(\boldsymbol{\Pi})}} \langle P_{\tau}\boldsymbol{u}_{c}, P_{\tau}\boldsymbol{u}_{c} \rangle$$

$$+ (\boldsymbol{f}(\boldsymbol{x}), \boldsymbol{u}_{c}) + (g(\boldsymbol{x}), p_{m}) + (h(\boldsymbol{x}), \boldsymbol{w}) \right]. \tag{2.22}$$

Utilizing integration by parts, and boundary conditions (2.16) and (2.17), we get the equality

$$((\boldsymbol{u}_c \cdot \nabla)\boldsymbol{v}, \boldsymbol{v}) + \frac{1}{2}((\nabla \cdot \boldsymbol{u}_c)\boldsymbol{v}, \boldsymbol{v}) = \frac{1}{2}\langle \boldsymbol{u}_c \cdot \boldsymbol{v}, \boldsymbol{v} \cdot \boldsymbol{n}_c \rangle, \ \forall \, \boldsymbol{v} \in [H_0^1(\Omega)]^d.$$
(2.23)

Due to the fact that

$$(w_c \nabla \phi_c, \mathbf{u}_c) + (w_m \nabla \phi_m, \mathbf{u}_m) = (\mathbf{u} \cdot \nabla \phi, w)$$
(2.24)

using (2.23), and collecting the similar terms, we transfer (2.22) into

$$2R\frac{dR}{dt} = \left(\frac{\partial \boldsymbol{u}_{c}}{\partial t}, \boldsymbol{u}_{c}\right) + \gamma \epsilon (\nabla \phi, \nabla \frac{\partial \phi}{\partial t}) + 2\epsilon_{2} \left(\frac{\partial p_{c}}{\partial t}, p_{c}\right) + \xi \frac{\gamma}{\epsilon} (f(\phi), \frac{\partial \phi}{\partial t})$$

$$-\left[-2\nu(\mathbb{D}(\boldsymbol{u}_{c}), \mathbb{D}(\boldsymbol{u}_{c})) + (p_{c}, \nabla \cdot \boldsymbol{u}_{c}) - \xi((\boldsymbol{u}_{c} \cdot \nabla)\boldsymbol{u}_{c}, \boldsymbol{u}_{c}) + \xi(\boldsymbol{w}_{c}\nabla\phi_{c}, \boldsymbol{u}_{c}) - \frac{\xi}{2} ((\nabla \cdot \boldsymbol{u}_{c})\boldsymbol{u}_{c}, \boldsymbol{u}_{c})\right]$$

$$-(\nabla \cdot \boldsymbol{u}_{c}, p_{c}) - (\mathbb{K}^{-1}\boldsymbol{u}_{m}, \boldsymbol{u}_{m}) - (\nabla p_{m}, \boldsymbol{u}_{m}) + \xi(\boldsymbol{w}_{m}\nabla\phi_{m}, \boldsymbol{u}_{m}) + (\boldsymbol{u}_{m}, \nabla p_{m}) - M(\nabla \boldsymbol{w}, \nabla \boldsymbol{w})$$

$$-\xi(\boldsymbol{u} \cdot \nabla \phi, \boldsymbol{w}) + (\boldsymbol{f}(\boldsymbol{x}), \boldsymbol{u}_{c}) + (g(\boldsymbol{x}), p_{m}) + (h(\boldsymbol{x}), \boldsymbol{w})d\boldsymbol{x}\right] + \xi \langle p_{m} - \frac{1}{2}|\boldsymbol{u}_{c}|^{2}, \boldsymbol{u}_{c} \cdot \boldsymbol{n}_{c} \rangle$$

$$-\xi \langle \boldsymbol{u}_{c} \cdot \boldsymbol{n}_{c}, p_{m} \rangle + \frac{\alpha\nu\sqrt{d}}{\sqrt{\text{trace}(\boldsymbol{\Pi})}} \langle P_{\tau}\boldsymbol{u}_{c}, P_{\tau}\boldsymbol{u}_{c} \rangle$$

$$+\xi \left[-2\nu(\mathbb{D}(\boldsymbol{u}_{c}), \mathbb{D}(\boldsymbol{u}_{c})) - (\mathbb{K}^{-1}\boldsymbol{u}_{m}, \boldsymbol{u}_{m}) - (M\nabla \boldsymbol{w}, \nabla \boldsymbol{w}) - \frac{\alpha\nu\sqrt{d}}{\sqrt{\text{trace}(\boldsymbol{\Pi})}} \langle P_{\tau}\boldsymbol{u}_{c}, P_{\tau}\boldsymbol{u}_{c} \rangle$$

$$+(\boldsymbol{f}(\boldsymbol{x}), \boldsymbol{u}_{c}) + (g(\boldsymbol{x}), p_{m}) + (h(\boldsymbol{x}), \boldsymbol{w})\right]$$

$$(2.25)$$

In sum, we reformulate the system (2.1)-(2.4), (2.5)-(2.8) into the following gPAV-based equivalent form

$$\frac{\partial \phi}{\partial t} + \xi \boldsymbol{u} \cdot \nabla \phi - \nabla \cdot (M(\phi)\nabla w) = h(\boldsymbol{x}), \tag{2.26}$$

$$w + \gamma \epsilon \triangle \phi - \xi \frac{\gamma}{\epsilon} f(\phi) = 0, \tag{2.27}$$

$$\mathbb{K}^{-1}\boldsymbol{u}_m + \nabla p_m - \xi w_m \nabla \phi_m = 0, \tag{2.28}$$

$$\nabla \cdot \boldsymbol{u}_m = g(\boldsymbol{x}), \tag{2.29}$$

$$\frac{\partial \boldsymbol{u}_c}{\partial t} + \xi (\boldsymbol{u}_c \cdot \nabla) \boldsymbol{u}_c - \nabla \cdot \mathbb{T}(\boldsymbol{u}_c, p_c) - \xi w_c \nabla \phi_c = \boldsymbol{f}(\boldsymbol{x}), \tag{2.30}$$

$$2\epsilon_2 \frac{\partial p_c}{\partial t} + \nabla \cdot \boldsymbol{u}_c = 0, \tag{2.31}$$

$$2R\frac{dR}{dt} = \left(\frac{\partial \boldsymbol{u}_{c}}{\partial t}, \boldsymbol{u}_{c}\right) + \gamma\epsilon(\nabla\phi, \nabla\frac{\partial\phi}{\partial t}) + 2\epsilon_{2}\left(\frac{\partial p_{c}}{\partial t}, p_{c}\right) + \xi\frac{\gamma}{\epsilon}\left(f(\phi), \frac{\partial\phi}{\partial t}\right)$$

$$-\left[-2\nu(\mathbb{D}(\boldsymbol{u}_{c}), \mathbb{D}(\boldsymbol{u}_{c})) + (p_{c}, \nabla \cdot \boldsymbol{u}_{c}) - \xi((\boldsymbol{u}_{c} \cdot \nabla)\boldsymbol{u}_{c}, \boldsymbol{u}_{c}) + \xi(\boldsymbol{w}_{c}\nabla\phi_{c}, \boldsymbol{u}_{c}) - \frac{\xi}{2}((\nabla \cdot \boldsymbol{u}_{c})\boldsymbol{u}_{c}, \boldsymbol{u}_{c})\right]$$

$$-(\nabla \cdot \boldsymbol{u}_{c}, p_{c}) - (\mathbb{K}^{-1}\boldsymbol{u}_{m}, \boldsymbol{u}_{m}) - (\nabla p_{m}, \boldsymbol{u}_{m}) + \xi(\boldsymbol{w}_{m}\nabla\phi_{m}, \boldsymbol{u}_{m}) + (\boldsymbol{u}_{m}, \nabla p_{m}) - M(\nabla \boldsymbol{w}, \nabla \boldsymbol{w})$$

$$-\xi(\boldsymbol{u} \cdot \nabla\phi, \boldsymbol{w}) + (\boldsymbol{f}(\boldsymbol{x}), \boldsymbol{u}_{c}) + (g(\boldsymbol{x}), p_{m}) + (h(\boldsymbol{x}), \boldsymbol{w})\right] + \xi\langle p_{m} - \frac{1}{2}|\boldsymbol{u}_{c}|^{2}, \boldsymbol{u}_{c} \cdot \boldsymbol{n}_{c}\rangle$$

$$-\xi\langle \boldsymbol{u}_{c} \cdot \boldsymbol{n}_{c}, p_{m}\rangle + \frac{\alpha\nu\sqrt{d}}{\sqrt{\mathrm{trace}(\boldsymbol{H})}}\langle P_{\tau}\boldsymbol{u}_{c}, P_{\tau}\boldsymbol{u}_{c}\rangle$$

$$+\xi\left[-2\nu(\mathbb{D}(\boldsymbol{u}_{c}), \mathbb{D}(\boldsymbol{u}_{c})) - (\mathbb{K}^{-1}\boldsymbol{u}_{m}, \boldsymbol{u}_{m}) - (M\nabla\boldsymbol{w}, \nabla\boldsymbol{w}) - \frac{\alpha\nu\sqrt{d}}{\sqrt{\mathrm{trace}(\boldsymbol{H})}}\langle P_{\tau}\boldsymbol{u}_{c}, P_{\tau}\boldsymbol{u}_{c}\rangle$$

$$+(\boldsymbol{f}(\boldsymbol{x}), \boldsymbol{u}_{c}) + (g(\boldsymbol{x}), p_{m}) + (h(\boldsymbol{x}), \boldsymbol{w})\right] + (1 - \xi)|(\boldsymbol{f}(\boldsymbol{x}), \boldsymbol{u}_{c}) + (g(\boldsymbol{x}), p_{m}) + (h(\boldsymbol{x}), \boldsymbol{w})|. \tag{2.32}$$

The term $|\cdot|$ denotes the absolute value.

2.3 The weak formulation

We now provide the weak formulation of the CHNSD model system (2.1)-(2.12). Define the space

$$\dot{L}^2(\Omega_j) := \{ v \in L^2(\Omega_j) : \int_{\Omega_j} v \, \mathrm{d}\boldsymbol{x} = 0 \}. \tag{2.33}$$

Then we denote $\dot{H}^1(\Omega_j) = H^1(\Omega_j) \cap \dot{L}^2(\Omega_j)$, which is a Hilbert space with inner product $(u, v)_{H^1} = \int_{\Omega_j} \nabla u \cdot \nabla v \, d\boldsymbol{x}$ due to the classical Poincaré inequality for functions with zero mean. Its dual space is simply denoted by $(\dot{H}^1(\Omega_j))'$. For our coupled system, the spaces that we utilize are

$$Y_j = H^1(\Omega_j), \quad Y = H^1(\Omega),$$
 $X_{j,div} = \{ \boldsymbol{v} \in X_j \mid \nabla \cdot \boldsymbol{v} = 0 \}, \quad j = c, m,$
 $X_c = \{ \boldsymbol{v} \in [H^1(\Omega_c)]^d \mid \boldsymbol{v} = 0 \text{ on } \Gamma_c \},$
 $X_m = \{ \boldsymbol{v} \in [H^1(\Omega_m)]^d \mid \boldsymbol{v} \cdot \boldsymbol{n}_m = 0 \text{ on } \Gamma_m \},$
 $Q_m = \dot{H}^1(\Omega_m), \quad Q_c = L^2(\Omega_c).$

 P_{τ} denotes the projection onto the tangent space on Γ , i.e. $P_{\tau} \boldsymbol{u} = \sum_{j=1}^{d-1} (\boldsymbol{u} \cdot \boldsymbol{\tau}_j) \boldsymbol{\tau}_j$. For the domain $\Omega_j (j=c,m), (\cdot,\cdot)$ denotes the L^2 inner product on the domain Ω_j decided by the subscript of integrated functions, and $\langle \cdot, \cdot \rangle$ denotes the L^2 inner product on the interface Γ . Then it is clear that

$$(u_m, v_m) = \int_{\Omega_m} u_m v_m d\mathbf{x}, \quad (u_c, v_c) = \int_{\Omega_c} u_c v_c d\mathbf{x}, \quad (u, v) = \int_{\Omega_m} u_m v_m d\mathbf{x} + \int_{\Omega_c} u_c v_c d\mathbf{x},$$
$$\|u_m\| := \left(\int_{\Omega_m} |u_m|^2 d\mathbf{x}\right)^{\frac{1}{2}}, \quad \|u_c\| := \left(\int_{\Omega_c} |u_c|^2 d\mathbf{x}\right)^{\frac{1}{2}}, \quad \|u\|^2 = \int_{\Omega_m} |u_m|^2 d\mathbf{x} + \int_{\Omega_c} |u_c|^2 d\mathbf{x},$$

where $u_m := u|_{\Omega_m}$ and $u_c := u|_{\Omega_c}$. We also denote H' the dual space of H with the duality induced by the L^2 inner product.

By applying the seven interface conditions (2.13)-(2.12) and integration of parts, we give the weak formulation of the proposed equivalent CHNSD system as follows: find

$$(\boldsymbol{u}_m, p_m, \boldsymbol{u}_c, p_c, \phi, w) \in (\boldsymbol{X}_m, Q_m, \boldsymbol{X}_c, Q_c, Y, Y)$$

such that

$$\left(\frac{\partial \phi}{\partial t}, \psi\right) + \xi(\boldsymbol{u} \cdot \nabla \phi, \psi) + (M(\phi)\nabla w, \nabla \psi) = (h(\boldsymbol{x}), \psi), \ \forall \psi \in Y,$$
(2.34)

$$(w,\omega) - \gamma \epsilon(\nabla \phi, \nabla \omega) - \xi \frac{\gamma}{\epsilon} (f(\phi), \omega) = 0, \ \forall \omega \in Y,$$
 (2.35)

$$(\boldsymbol{u}_m, \boldsymbol{v}) + \mathbb{K}(\nabla p_m, \boldsymbol{v}) - \xi \mathbb{K}(w_m \nabla \phi_m, \boldsymbol{v}) = 0, \ \forall \, \boldsymbol{v} \in \boldsymbol{X}_m,$$

$$(2.36)$$

$$-(\boldsymbol{u}_m, \nabla q) - \xi \langle \boldsymbol{u}_c \cdot \boldsymbol{n}_c, q \rangle = (g(\boldsymbol{x}), q), \ \forall \ q \in Q_m,$$

$$(2.37)$$

$$(\frac{\partial \boldsymbol{u}_c}{\partial t}, \boldsymbol{v}) + \xi \left(\left(\boldsymbol{u}_c \cdot \nabla \right) \boldsymbol{u}_c, \boldsymbol{v} \right) + \frac{\xi}{2} \left(\left(\nabla \cdot \boldsymbol{u}_c \right) \boldsymbol{u}_c, \boldsymbol{v} \right) + \left(2\nu \mathbb{D}(\boldsymbol{u}_c), \mathbb{D}(\boldsymbol{v}) \right) - \left(p_c, \nabla \cdot \boldsymbol{v} \right) - \xi (w_c \nabla \phi_c, \boldsymbol{v})$$

$$+\xi \langle p_m - \frac{1}{2} | \boldsymbol{u}_c |^2, \boldsymbol{v} \cdot \boldsymbol{n}_c \rangle + \frac{\alpha \nu \sqrt{d}}{\sqrt{\operatorname{trace}(\boldsymbol{\Pi})}} \langle P_{\tau} \boldsymbol{u}_c, P_{\tau} \boldsymbol{v} \rangle = (\boldsymbol{f}(\boldsymbol{x}), \boldsymbol{v}), \ \forall \, \boldsymbol{v} \in \boldsymbol{X}_c,$$
(2.38)

$$2\epsilon_{2}(\frac{\partial p_{c}}{\partial t}, q) + (\nabla \cdot \boldsymbol{u}_{c}, q) = 0, \ \forall q \in Q_{c},$$

$$2R\frac{dR}{dt} = (\frac{\partial \boldsymbol{u}_{c}}{\partial t}, \boldsymbol{u}_{c}) + \gamma \epsilon (\nabla \phi, \nabla \frac{\partial \phi}{\partial t}) + 2\epsilon_{2}(\frac{\partial p_{c}}{\partial t}, p_{c}) + \xi \frac{\gamma}{\epsilon} (f(\phi), \frac{\partial \phi}{\partial t})$$

$$- \left[-2\nu \| \mathbb{D}(\boldsymbol{u}_{c}) \|^{2} + (p_{c}, \nabla \cdot \boldsymbol{u}_{c}) - \xi ((\boldsymbol{u}_{c} \cdot \nabla)\boldsymbol{u}_{c}, \boldsymbol{u}_{c}) + \xi (\boldsymbol{w}_{c} \nabla \phi_{c}, \boldsymbol{u}_{c}) - \frac{\xi}{2} ((\nabla \cdot \boldsymbol{u}_{c})\boldsymbol{u}_{c}, \boldsymbol{u}_{c}) \right]$$

$$- (\nabla \cdot \boldsymbol{u}_{c}, p_{c}) - \mathbb{K}^{-1} \| \boldsymbol{u}_{m} \|^{2} - (\nabla p_{m}, \boldsymbol{u}_{m}) + \xi (\boldsymbol{w}_{m} \nabla \phi_{m}, \boldsymbol{u}_{m}) + (\boldsymbol{u}_{m}, \nabla p_{m}) - M \| \nabla \boldsymbol{w} \|^{2}$$

$$- \xi (\boldsymbol{u} \cdot \nabla \phi, \boldsymbol{w}) + (\boldsymbol{f}(\boldsymbol{x}), \boldsymbol{u}_{c}) + (g(\boldsymbol{x}), p_{m}) + (h(\boldsymbol{x}), \boldsymbol{w}) + \xi (p_{m} - \frac{1}{2} |\boldsymbol{u}_{c}|^{2}, \boldsymbol{u}_{c} \cdot \boldsymbol{n}_{c})$$

$$- \xi \langle \boldsymbol{u}_{c} \cdot \boldsymbol{n}_{c}, p_{m} \rangle + \frac{\alpha \nu \sqrt{d}}{\sqrt{\operatorname{trace}(\boldsymbol{\Pi})}} \langle P_{\tau} \boldsymbol{u}_{c}, P_{\tau} \boldsymbol{u}_{c} \rangle$$

$$+\xi \left[-2\nu \|\mathbb{D}(\boldsymbol{u}_c)\|^2 - \mathbb{K}^{-1} \|\boldsymbol{u}_m\|^2 - M \|\nabla w\|^2 - \frac{\alpha\nu\sqrt{d}}{\sqrt{\text{trace}(\boldsymbol{\Pi})}} \langle P_{\tau}\boldsymbol{u}_c, P_{\tau}\boldsymbol{u}_c \rangle + (\boldsymbol{f}(\boldsymbol{x}), \boldsymbol{u}_c) \right.$$
$$\left. + (g(\boldsymbol{x}), p_m) + (h(\boldsymbol{x}), w) \right] + (1 - \xi) |(\boldsymbol{f}(\boldsymbol{x}), \boldsymbol{u}_c) + (g(\boldsymbol{x}), p_m) + (h(\boldsymbol{x}), w)|,$$
(2.40)

where $t \in [0,T]$, T is a finite time, $\boldsymbol{u}_m \in L^{\infty}(0,T;[L^2(\Omega_m)]^d) \cap L^2(0,T;\boldsymbol{X}_m)$, $\boldsymbol{u}_c \in L^{\infty}(0,T;[L^2(\Omega_c)]^d) \cap L^2(0,T;\boldsymbol{X}_{c,div})$, $\frac{\partial \boldsymbol{u}_c}{\partial t} \in L^2(0,T;\boldsymbol{X}'_{c,div})$, $p_j \in L^2(0,T;Q_j)$, $j = \{c,m\}$, $\phi \in L^{\infty}(0,T;Y) \cap L^2(0,T;H^3(\Omega))$, $\frac{\partial \phi}{\partial t} \in L^2(0,T;Y')$, $w \in L^2(0,T;Y)$.

It is remarkable that the above weak formulation satisfies the dissipative energy law with the total energy of the coupled system (2.34)-(2.40) as follows

$$\mathcal{E}(t) = |R|^2. \tag{2.41}$$

Lemma 1 Let $(\mathbf{u}_m, \mathbf{u}_c, \phi_m, \phi_c, w_m, w_c)$ be a smooth solution to the initial boundary value problem (2.1)-(2.18). Then $(\mathbf{u}_m, \mathbf{u}_c, \phi_m, \phi_c, w_m, w_c)$ satisfies the following basic energy law:

$$\frac{d}{dt}\mathcal{E} = -\xi \mathcal{D}(t) - \xi \left[(\boldsymbol{f}(\boldsymbol{x}), \boldsymbol{u}_c) + (g(\boldsymbol{x}), p_m) + (h(\boldsymbol{x}), w) \right] + (1 - \xi) \left| (\boldsymbol{f}(\boldsymbol{x}), \boldsymbol{u}_c) + (g(\boldsymbol{x}), p_m) + (h(\boldsymbol{x}), w) \right|,$$
(2.42)

where the energy dissipation \mathcal{D} is given by

$$\mathcal{D}(t) = \|\sqrt{2\nu}\mathbb{D}(\boldsymbol{u}_c)\|^2 + \|\sqrt{\mathbb{K}^{-1}}\boldsymbol{u}_m\|^2 + \|\sqrt{M(\phi)}\nabla w\|^2 + \frac{\alpha\nu\sqrt{d}}{\sqrt{trace(\Pi)}}\langle P_{\tau}\boldsymbol{u}_c, P_{\tau}\boldsymbol{u}_c\rangle. \tag{2.43}$$

This implies an energy-stable feature under the assumption of zero source terms f(x), g(x), and h(x).

Proof.

First, for the Cahn-Hilliard equation, we choose $\psi = w$ and $\omega = -\frac{\partial \phi}{\partial t}$ in (2.34) and (2.35), respectively, and add these two equations to derive

$$\gamma \epsilon(\nabla \phi, \nabla \frac{\partial \phi}{\partial t}) + \xi \frac{\gamma}{\epsilon} (f(\phi), \frac{\partial \phi}{\partial t}) + \xi M \|\nabla w\|^2 + \xi (\boldsymbol{u} \cdot \nabla \phi, w) = 0.$$
 (2.44)

Next, we consider the matrix part. By setting $q = p_m$ and $\mathbf{v} = \mathbf{u}_m$ in (2.37) and (2.36), respectively, and taking the summation, we obtain

$$\|\sqrt{\mathbb{K}^{-1}}\boldsymbol{u}_m\|^2 - \xi(w_m \nabla \phi_m, \boldsymbol{u}_m) - \xi \langle \boldsymbol{u}_c \cdot \boldsymbol{n}_c, p_m \rangle = 0.$$
 (2.45)

For the conduit part, taking the test function in (2.38) and (2.39) by $\mathbf{v} = \mathbf{u}_c$ and $q = p_c$, adding the resultants together, we get

$$\left(\frac{\partial \boldsymbol{u}_{c}}{\partial t}, \boldsymbol{u}_{c}\right) + \xi\left((\boldsymbol{u}_{c} \cdot \nabla)\boldsymbol{u}_{c}, \boldsymbol{u}_{c}\right) + \|\sqrt{2\nu}\mathbb{D}(\boldsymbol{u}_{c})\|^{2} + \frac{\xi}{2}\left((\nabla \cdot \boldsymbol{u}_{c})\boldsymbol{u}_{c}, \boldsymbol{u}_{c}\right) - (p_{c}, \nabla \cdot \boldsymbol{u}_{c}) - \xi(w_{c}\nabla\phi_{c}, \boldsymbol{v}) + \epsilon_{2}\left(\frac{\partial p_{c}}{\partial t}, p\right) + (\nabla \cdot \boldsymbol{u}_{c}, p) + \xi\langle p_{m} - \frac{1}{2}|\boldsymbol{u}_{c}|^{2}, \boldsymbol{u}_{c} \cdot \boldsymbol{n}_{c}\rangle + \frac{\alpha\sqrt{d}}{\sqrt{\operatorname{trace}(\boldsymbol{\Pi})}}\langle \nu P_{\tau}\boldsymbol{u}_{c}, P_{\tau}\boldsymbol{u}_{c}\rangle = 0. \tag{2.46}$$

To sum up of (2.40), (2.44), (2.46) and (2.45), we obtain

$$\frac{d}{dt}|R|^{2} = -\xi \left[\|\sqrt{2\nu}\mathbb{D}(\boldsymbol{u}_{c})\|^{2} + \|\sqrt{\mathbb{K}^{-1}}\boldsymbol{u}_{m}\|^{2} + M\|\nabla w\|^{2} + \frac{\alpha\sqrt{d}}{\sqrt{\operatorname{trace}(\boldsymbol{\Pi})}} \langle \nu P_{\tau}\boldsymbol{u}_{c}, P_{\tau}\boldsymbol{u}_{c} \rangle \right. \\
\left. - (\boldsymbol{f}(\boldsymbol{x}), \boldsymbol{u}_{c}) - (g(\boldsymbol{x}), p_{m}) - (h(\boldsymbol{x}), w) \right] + (1 - \xi)|(\boldsymbol{f}(\boldsymbol{x}), \boldsymbol{u}_{c}) + (g(\boldsymbol{x}), p_{m}) + (h(\boldsymbol{x}), w)|, \tag{2.47}$$

which implies that the energy of weak formulation is non-increasing (2.42) under the zero source terms. This completes the proof of Lemma 1.

3 Second order numerical schemes

In this section, we present the second-order fully discrete schemes for the weak formulation (2.34)-(2.40) using finite element method for spatial discretization.

Let \mathfrak{F}_h be a quasi-uniform mesh of size h for the domain Ω . We introduce the finite element approximation spaces Y_h , Y_{jh} , X_{jh} and Q_{jh} of Y, Y_j , X_j and Q_j . Further, we assume the X_{ch} and Q_{ch} are stable pairs satisfying

$$\inf_{0 \neq q_h} \sup_{0 \neq \boldsymbol{v}_h} \frac{(\nabla \cdot \boldsymbol{v}_h, q_h)}{\|\boldsymbol{v}_h\|_1} > C \|q_h\|, \ \forall q_h \in Q_{ch}, \boldsymbol{v}_h \in \boldsymbol{X}_{ch},$$
(3.1)

 X_{mh} and Q_{mh} are stable in the sense that

$$\inf_{0 \neq q_h} \sup_{0 \neq \boldsymbol{v}_h} \frac{(\nabla \cdot \boldsymbol{v}_h, q_h)}{\|\boldsymbol{v}_h\|} > C \|q_h\|, \ \forall q_h \in Q_{mh}, \boldsymbol{v}_h \in \boldsymbol{X}_{mh}.$$
(3.2)

Then the semi-discretization of the system (2.37)-(2.35) is to find

$$(u_{mh}, p_{mh}, u_{ch}, p_{ch}, \phi_h, w_h) \in (X_{mh}, Q_{mh}, X_{ch}, Q_{ch}, Y_h, Y_h)$$

such that

$$\left(\frac{\partial \phi_h}{\partial t}, \psi_h\right) + \xi(\boldsymbol{u}_h \cdot \nabla \phi_h, \psi_h) + \left(M(\phi_h) \nabla w_h, \nabla \psi_h\right) = (h(\boldsymbol{x}), \psi_h), \ \forall \, \psi_h \in Y_h,$$
(3.3)

$$(w_h, \omega_h) - \gamma \epsilon(\nabla \phi_h, \nabla \omega_h) - \xi \frac{\gamma}{\epsilon} (f(\phi_h), \omega_h) = 0, \ \forall \omega_h \in Y_h,$$

$$(3.4)$$

$$(\boldsymbol{u}_{mh}, \boldsymbol{v}_h) + \mathbb{K}(\nabla p_{mh}, \boldsymbol{v}_h) - \xi \mathbb{K}(w_{mh} \nabla \phi_{mh}, \boldsymbol{v}_h) = 0, \ \forall \, \boldsymbol{v}_h \in \boldsymbol{X}_{mh},$$
(3.5)

$$-(\boldsymbol{u}_{mh}, \nabla q_h) - \xi \langle \boldsymbol{u}_{ch} \cdot \boldsymbol{n}_c, q_h \rangle = (g(\boldsymbol{x}), q_h), \ \forall q_h \in Q_m,$$

$$(3.6)$$

$$(\frac{\partial \boldsymbol{u}_{ch}}{\partial t},\boldsymbol{v}_h) + \xi \left(\left(\boldsymbol{u}_{ch} \cdot \nabla \right) \boldsymbol{u}_{ch}, \boldsymbol{v}_h \right) + \frac{\xi}{2} \left(\left(\nabla \cdot \boldsymbol{u}_{ch} \right) \boldsymbol{u}_{ch}, \boldsymbol{v}_h \right) + \left(2\nu \mathbb{D}(\boldsymbol{u}_{ch}), \mathbb{D}(\boldsymbol{v}_h) \right) - \left(p_{ch}, \nabla \cdot \boldsymbol{v}_h \right)$$

$$-\xi(w_{ch}\nabla\phi_{ch}, \boldsymbol{v}_h) + \xi\langle p_{mh} - \frac{1}{2}|\boldsymbol{u}_{ch}|^2, \boldsymbol{v}_h \cdot \boldsymbol{n}_c \rangle + \frac{\alpha\nu\sqrt{d}}{\sqrt{\text{trace}(\boldsymbol{\Pi})}}\langle P_{\tau}\boldsymbol{u}_{ch}, P_{\tau}\boldsymbol{v}_h \rangle$$

$$= (\boldsymbol{f}(\boldsymbol{x}), \boldsymbol{v}_h), \forall \boldsymbol{v}_h \in \boldsymbol{X}_{ch},$$
(3.7)

$$2\epsilon_{2}(\frac{\partial p_{ch}}{\partial t}, q_{h}) + (\nabla \cdot \boldsymbol{u}_{ch}, q_{h}) = 0, \ \forall q_{h} \in Q_{ch},$$

$$2R\frac{dR}{dt} = (\frac{\partial \boldsymbol{u}_{ch}}{\partial t}, \boldsymbol{u}_{ch}) + \gamma \epsilon (\nabla \phi_{h}, \nabla \frac{\partial \phi_{h}}{\partial t}) + 2\epsilon_{2}(\frac{\partial p_{ch}}{\partial t}, p_{ch}) + \xi \frac{\gamma}{\epsilon} (f(\phi_{h}), \frac{\partial \phi_{h}}{\partial t})$$

$$+ \left[2\nu \|\mathbb{D}(\boldsymbol{u}_{ch})\|^{2} - (p_{ch}, \nabla \cdot \boldsymbol{u}_{ch}) + \xi ((\boldsymbol{u}_{ch} \cdot \nabla)\boldsymbol{u}_{ch}, \boldsymbol{u}_{ch}) - \xi (w_{c}\nabla \phi_{ch}, \boldsymbol{u}_{ch}) + (\nabla \cdot \boldsymbol{u}_{ch}, p_{ch}) \right]$$
(3.8)

$$+rac{\xi}{2}((
abla\cdotoldsymbol{u}_{ch},oldsymbol{u}_{ch},oldsymbol{u}_{ch})+\xi((oldsymbol{u}_{ch},oldsymbol{u}_{ch},oldsymbol{u}_{ch})+(
ablaoldsymbol{u}_{ch},oldsymbol{p}_{ch})+ \mathbb{K}^{-1}\|oldsymbol{u}_{mh}\|^2+(
abla p_{mh},oldsymbol{u}_{mh})-\xi(w_{mh}
abla\phi_{mh},oldsymbol{u}_{mh})-(oldsymbol{u}_{mh},
abla p_{mh})$$

$$+M\|\nabla w_h\|^2 + \xi(\boldsymbol{u}_h \cdot \nabla \phi_h, w_h) - (\boldsymbol{f}(\boldsymbol{x}), \boldsymbol{u}_{ch}) - (g(\boldsymbol{x}), p_{mh}) - (h(\boldsymbol{x}), w_h)$$

$$+\xi \langle p_{mh} - \frac{1}{2} | \boldsymbol{u}_{ch} |^2, \boldsymbol{u}_{ch} \cdot \boldsymbol{n}_c \rangle - \xi \langle \boldsymbol{u}_{ch} \cdot \boldsymbol{n}_c, p_{mh} \rangle + \frac{\alpha \nu \sqrt{\mathrm{d}}}{\sqrt{\mathrm{trace}(\prod)}} \langle P_{\tau} \boldsymbol{u}_{ch}, P_{\tau} \boldsymbol{u}_{ch} \rangle$$

$$+\xi \Big[-2\nu \|\mathbb{D}(\boldsymbol{u}_{ch})\|^2 - \mathbb{K}^{-1} \|\boldsymbol{u}_{mh}\|^2 - M \|\nabla w_h\|^2 - \frac{\alpha\nu\sqrt{\mathrm{d}}}{\sqrt{\mathrm{trace}(\prod)}} \langle P_{\tau}\boldsymbol{u}_{ch}, P_{\tau}\boldsymbol{u}_{ch} \rangle + (\boldsymbol{f}(\boldsymbol{x}), \boldsymbol{u}_{ch}) \Big]$$

+
$$(g(\mathbf{x}), p_{mh}) + (h(\mathbf{x}), w_h)$$
] + $(1 - \xi)|(\mathbf{f}(\mathbf{x}), \mathbf{u}_{ch}) + (g(\mathbf{x}), p_{mh}) + (h(\mathbf{x}), w_h)|.$ (3.9)

Let $0 = t_0 < t_1 < \cdots < t_M = T$ be a uniform partition of [0, T] into subintervals $J^n = (t_n, t_{n+1})$, $n = 0, 1, \ldots, M - 1$, $\Delta t = t_{n+1} - t_n = \frac{T}{M}$ be time step size. Then we develop the following second order accuracy in time, decoupled, linearized and unconditionally stable full discretization.

3.1 Decoupled energy-stable gPAV-CNLF numerical scheme

Denoting

$$\hat{v}^{n+1} = \frac{v^{n+1} + v^{n-1}}{2}, \quad \overline{v}^{n+1} = \frac{\breve{v}^{n+1} + v^{n-1}}{2}, \tag{3.10}$$

$$\xi^{n+1} = \frac{(R^{n+1})^2}{E(\overline{\boldsymbol{u}}_{ch}^{n+1}, \overline{\phi}_h^{n+1})},\tag{3.11}$$

where \check{v}^{n+1} is the second-order approximation of v^{n+1} to be defined later (more details are presented in (4.4) of Section 4.1).

The Crank-Nicolson Leap-Frog artificial compression (gPAV-CNLF) method is as follows:

Step 1: Find $(\phi_h^{n+1}, w_h^{n+1}) \in Y_h \times Y_h$, such that for all $(\psi_h, \omega_h) \in Y_h \times Y_h$

$$\left(\frac{\phi_h^{n+1} - \phi_h^{n-1}}{2\Delta t}, \psi_h\right) + \xi^{n+1}(\boldsymbol{u}_h^n \cdot \nabla \phi_h^n, \psi_h) + \left(M(\phi_h^n) \nabla \widehat{w}_h^{n+1}, \nabla \psi_h\right) = (h(\boldsymbol{x}), \psi_h), \tag{3.12}$$

$$(\widehat{w}_h^{n+1}, \omega_h) - \gamma \epsilon (\nabla \widehat{\phi}_h^{n+1}, \nabla \omega_h) - \xi^{n+1} \frac{\gamma}{\epsilon} (f(\phi_h^n), \omega_h) - S(\phi_h^{n+1} - \phi_h^{n-1}, \omega_h) = 0, \tag{3.13}$$

where S is a positive stabilized parameter, and

$$\boldsymbol{u}_{h}^{n} := \begin{cases} \boldsymbol{u}_{ch}^{n}, & \boldsymbol{x} \in \Omega_{c}, \\ \boldsymbol{u}_{mh}^{n}, & \boldsymbol{x} \in \Omega_{m}. \end{cases}$$

$$(3.14)$$

Step 2: Find $(\boldsymbol{u}_{mh}^{n+1}, p_{mh}^{n+1}) \in \boldsymbol{X}_{mh} \times Q_{mh}$, such that for all $(\boldsymbol{v}_h, q_h) \in \boldsymbol{X}_{mh} \times Q_{mh}$

$$\mathbb{K}^{-1}(\boldsymbol{u}_{mh}^{n+1}, \boldsymbol{v}_h) + (\nabla \widehat{p}_{mh}^{n+1}, \boldsymbol{v}_h) - \xi^{n+1}(\boldsymbol{w}_{mh}^n \nabla \phi_{mh}^n, \boldsymbol{v}_h) + \beta_1 h(\nabla (\boldsymbol{u}_{mh}^{n+1} - \boldsymbol{u}_{mh}^{n-1}), \nabla \boldsymbol{v}_h) = 0, \quad (3.15)$$
$$-(\nabla \boldsymbol{u}_{mh}^{n+1}, \nabla q) - \xi^{n+1} \langle \boldsymbol{u}_{ch}^n \cdot \boldsymbol{n}_c, q_h \rangle = (g(\boldsymbol{x}), q_h), \quad (3.16)$$

where β_1 is a positive parameter to be specified later. Step 3: Find $u_{ch}^{n+1} \in X_{ch}$, such that for all $v_h \in X_{ch}$

$$\left(\frac{\boldsymbol{u}_{ch}^{n+1} - \boldsymbol{u}_{ch}^{n-1}}{2\Delta t}, \boldsymbol{v}_{h}\right) + \xi^{n+1} \left(\left(\boldsymbol{u}_{ch}^{n} \cdot \nabla\right) \boldsymbol{u}_{ch}^{n}, \boldsymbol{v}_{h}\right) + \frac{\xi^{n+1}}{2} \left(\left(\nabla \cdot \boldsymbol{u}_{ch}^{n}\right) \boldsymbol{u}_{ch}^{n}, \boldsymbol{v}\right) + 2\nu \left(\mathbb{D}(\widehat{\boldsymbol{u}}_{ch}^{n+1}), \mathbb{D}(\boldsymbol{v}_{h})\right) \\
+ \beta_{2} h \left(\nabla \left(\boldsymbol{u}_{ch}^{n+1} - \boldsymbol{u}_{ch}^{n-1}\right), \nabla \boldsymbol{v}_{h}\right) - \xi^{n+1} \left(\boldsymbol{w}_{ch}^{n} \nabla \phi_{ch}^{n}, \boldsymbol{v}_{h}\right) - \left(p_{ch}^{n}, \nabla \cdot \boldsymbol{v}_{h}\right) + \xi^{n+1} \left\langle p_{mh}^{n}, \boldsymbol{v}_{h} \cdot \boldsymbol{n}_{c}\right\rangle \\
- \frac{\xi^{n+1}}{2} \left\langle \boldsymbol{u}_{ch}^{n} \cdot \boldsymbol{u}_{ch}^{n}, \boldsymbol{v}_{h} \cdot \boldsymbol{n}_{c}\right\rangle + \frac{\alpha\nu\sqrt{d}}{\sqrt{\operatorname{trace}(\prod)}} \left\langle P_{\tau} \widehat{\boldsymbol{u}}_{ch}^{n+1}, P_{\tau} \boldsymbol{v}_{h}\right\rangle = (f(\boldsymbol{x}), \boldsymbol{v}_{h}), \tag{3.17}$$

where β_2 is a positive parameter.

Step 4: Find $p_{ch}^{n+1} \in Q_{ch}$, such that for all $q_h \in Q_{ch}$

$$\delta \Delta t(p_{ch}^{n+1} - p_{ch}^{n-1}, q_h) + (\nabla \cdot \boldsymbol{u}_{ch}^n, q_h) = 0.$$
(3.18)

Step 5: Find R^{n+1} , such that

$$\begin{split} &\frac{(R^{n+1})^2 - (R^{n-1})^2}{2\Delta t} = (\frac{\boldsymbol{u}_{ch}^{n+1} - \boldsymbol{u}_{ch}^{n-1}}{2\Delta t}, \widehat{\boldsymbol{u}}_{ch}^{n+1}) + \gamma \epsilon (\nabla \widehat{\phi}_{h}^{n+1}, \nabla \frac{\phi_{h}^{n+1} - \phi_{h}^{n-1}}{2\Delta t}) + 2\delta \Delta t^2 (\frac{p_{ch}^{n+1} - p_{ch}^{n-1}}{2\Delta t}, \widehat{p}_{ch}^{n+1}) \\ &+ \xi^{n+1} \frac{\gamma}{\epsilon} (f(\phi_{h}^{n}), \nabla \frac{\phi_{h}^{n+1} - \phi_{h}^{n-1}}{2\Delta t}) + S(\phi_{h}^{n+1} - \phi_{h}^{n-1}, \frac{\phi_{h}^{n+1} - \phi_{h}^{n-1}}{2}) + \beta_{1} h (\nabla (\boldsymbol{u}_{mh}^{n+1} - \boldsymbol{u}_{mh}^{n-1}), \nabla \widehat{\boldsymbol{u}}_{mh}^{n+1}) \\ &+ \beta_{2} h (\nabla (\boldsymbol{u}_{ch}^{n+1} - \boldsymbol{u}_{ch}^{n-1}), \nabla \widehat{\boldsymbol{u}}_{ch}^{n+1}) \\ &+ \left[2\nu \| \mathbb{D}(\widehat{\boldsymbol{u}}_{ch}^{n+1}) \|^{2} - (p_{ch}^{n}, \nabla \cdot \widehat{\boldsymbol{u}}_{ch}^{n+1}) + (\nabla \widehat{\boldsymbol{p}}_{mh}^{n+1}, \widehat{\boldsymbol{u}}_{mh}^{n+1}) + \mathbb{K}^{-1} \| \widehat{\boldsymbol{u}}_{mh}^{n+1} \|^{2} + \xi^{n+1} ((\boldsymbol{u}_{ch}^{n} \cdot \nabla) \boldsymbol{u}_{ch}^{n}, \widehat{\boldsymbol{u}}_{ch}^{n+1}) \\ &- \xi^{n+1} (\boldsymbol{w}_{ch}^{n} \nabla \phi_{ch}^{n}, \widehat{\boldsymbol{u}}_{ch}^{n+1}) + (\nabla \cdot \boldsymbol{u}_{ch}^{n}, \widehat{p}_{ch}^{n+1}) + \frac{\xi^{n+1}}{2} ((\nabla \cdot \boldsymbol{u}_{ch}^{n}) \boldsymbol{u}_{ch}^{n}, \widehat{\boldsymbol{u}}_{ch}^{n+1}) - \xi^{n+1} (\boldsymbol{w}_{mh}^{n} \nabla \phi_{mh}^{n}, \widehat{\boldsymbol{u}}_{mh}^{n+1}) \\ &- (\widehat{\boldsymbol{u}}_{mh}^{n+1}, \nabla \widehat{\boldsymbol{p}}_{mh}^{n+1}) + \| \sqrt{M(\phi_{h}^{n})} \nabla \widehat{\boldsymbol{w}}_{h}^{n+1} \|^{2} + \xi^{n+1} (\boldsymbol{u}_{h}^{n} \cdot \nabla \phi_{h}^{n}, \widehat{\boldsymbol{w}}_{h}^{n+1}) \\ &- (f(\boldsymbol{x}), \widehat{\boldsymbol{u}}_{ch}^{n+1}) - (g(\boldsymbol{x}), \widehat{p}_{mh}^{n+1}) - (h(\boldsymbol{x}), \widehat{\boldsymbol{w}}_{h}^{n+1}) \Big] \\ &+ \xi^{n+1} \langle p_{mh}^{n} - \frac{1}{2} |\boldsymbol{u}_{ch}^{n}|^{2}, \widehat{\boldsymbol{u}}_{ch}^{n+1} \cdot \boldsymbol{n}_{c} \rangle - \xi^{n+1} \langle \boldsymbol{u}_{ch}^{n} \cdot \boldsymbol{n}_{c}, \widehat{p}_{mh}^{n+1} \rangle + \frac{\alpha \nu \sqrt{d}}{\sqrt{\text{trace}(\prod)}} \langle P_{\tau} \widehat{\boldsymbol{u}}_{ch}^{n+1}, P_{\tau} \widehat{\boldsymbol{u}}_{ch}^{n+1} \rangle \\ &+ \xi^{n+1} [-2\nu \| \mathbb{D}(\overline{\boldsymbol{u}}_{ch}^{n+1}) \|^{2} - \mathbb{K}^{-1} \| \overline{\boldsymbol{u}}_{mh}^{n+1} \|^{2} - \| \sqrt{M(\overline{\phi}_{h}^{n})} \nabla \overline{\boldsymbol{w}}_{h}^{n+1} \|^{2} - \frac{\alpha \nu \sqrt{d}}{\sqrt{\text{trace}(\prod)}} \langle P_{\tau} \overline{\boldsymbol{u}}_{ch}^{n+1}, P_{\tau} \overline{\boldsymbol{u}}_{ch}^{n+1} \rangle] \\ &+ \xi^{n+1} S_{0} + (1 - \xi^{n+1}) |S_{0}|, \end{split}{3.19}$$

where

$$S_0 = (\boldsymbol{f}(\boldsymbol{x}), \overline{\boldsymbol{u}}_{ch}^{n+1}) + (g(\boldsymbol{x}), \overline{p}_{mh}^{n+1}) + (h(\boldsymbol{x}), \overline{\boldsymbol{w}}_{h}^{n+1}), \tag{3.20}$$

 $\overline{\boldsymbol{u}}_{ch}^{n+1},\,\overline{\boldsymbol{u}}_{mh}^{n+1},\,\overline{p}_{ch}^{n+1},\,\text{and}\,\,\overline{\boldsymbol{w}}_{h}^{n+1}\,\,\text{are second order approximations of}\,\,\boldsymbol{\widehat{u}}_{ch}^{n+1},\,\boldsymbol{\widehat{u}}_{mh}^{n+1},\,\boldsymbol{\widehat{p}}_{ch}^{n+1}\,\,\text{and}\,\,\boldsymbol{\widehat{w}}_{h}^{n+1}.$

Remark 1 Following the technique of artificial viscosity stabilization [39, 42], a term $-\beta h \triangle (\boldsymbol{u}_{ch}^{n+1} - \boldsymbol{u}_{ch}^{n-1})$ in (3.17) is introduced to improve the accuracy of gPAV schemes, particularly for high Reynolds number flows. The stabilized gPAV algorithm has accuracy $O(\Delta t^2 + h \Delta t + \text{spatial error})$.

In order to prove the energy stability of the CNLF numerical scheme, we first establish the following identity.

Theorem 1 The approximation $(\boldsymbol{u}_{mh}^{n+1}, \boldsymbol{u}_{ch}^{n+1}, p_{ch}^{n+1}, \phi_h^{n+1})$ by the scheme (3.12)-(3.19) satisfies the following equality:

$$\frac{1}{2}|R^{n+1}|^2 - \frac{1}{2}|R^{n-1}|^2 = -\xi^{n+1}\Delta t \left[\mathcal{D}^{n+1} - S_0\right] + \Delta t (1 - \xi^{n+1})|S_0|, \tag{3.21}$$

where \mathcal{D}^{n+1} is given by

$$\mathcal{D}^{n+1} = 2\nu \|\mathbb{D}(\overline{\boldsymbol{u}}_{ch}^{n+1})\|^2 + \|\sqrt{\mathbb{K}^{-1}}\overline{\boldsymbol{u}}_{mh}^{n+1}\|^2 + \|\sqrt{M(\phi_h^n)}\nabla \overline{\boldsymbol{w}}_h^{n+1}\|^2 + \frac{\alpha\nu\sqrt{d}}{\sqrt{trace(\prod)}}\langle P_{\tau}\overline{\boldsymbol{u}}_{ch}^{n+1}, P_{\tau}\overline{\boldsymbol{u}}_{ch}^{n+1}\rangle.$$
(3.22)

Hence the scheme is well-defined with $\xi^{n+1} > 0$.

Proof. Taking $\psi_h = \Delta t \widehat{w}_h^{n+1}$ and $\omega_h = -\frac{\phi_h^{n+1} - \phi_h^{n-1}}{2}$ in (3.12) and (3.13), respectively, adding these resultants, we derive

$$\gamma \epsilon (\nabla \widehat{\phi}_{h}^{n+1}, \nabla \frac{\phi_{h}^{n+1} - \phi_{h}^{n-1}}{2}) + \xi^{n+1} \frac{\gamma}{\epsilon} (f(\phi_{h}^{n}), \frac{\phi_{h}^{n+1} - \phi_{h}^{n-1}}{2}) + \Delta t \xi^{n+1} (\mathbf{u}_{h}^{n} \cdot \nabla \phi_{h}^{n}, \widehat{w}_{h}^{n+1}) \\
+ S(\phi_{h}^{n+1} - \phi_{h}^{n-1}, \frac{\phi_{h}^{n+1} - \phi_{h}^{n-1}}{2}) + \Delta t (M(\phi_{h}^{n}) \nabla \widehat{w}_{h}^{n+1}, \nabla \widehat{w}_{h}^{n+1}) = 0.$$
(3.23)

Next, we consider the conduit part. Taking the test function $\mathbf{v}_h = \Delta t \hat{\mathbf{u}}_{ch}^{n+1}$ in (3.17), and $q_h = \hat{p}_{ch}^{n+1}$ in (3.18), respective, we take the sum to obtain

$$\left(\frac{\boldsymbol{u}_{ch}^{n+1} - \boldsymbol{u}_{ch}^{n-1}}{2}, \widehat{\boldsymbol{u}}_{ch}^{n+1}\right) + \xi^{n+1} \Delta t \left(\left(\boldsymbol{u}_{ch}^{n} \cdot \nabla\right) \boldsymbol{u}_{ch}^{n}, \widehat{\boldsymbol{u}}_{ch}^{n+1}\right) + \Delta t \frac{\xi^{n+1}}{2} \left(\left(\nabla \cdot \boldsymbol{u}_{ch}^{n}\right) \boldsymbol{u}_{ch}^{n}, \widehat{\boldsymbol{u}}_{ch}^{n+1}\right) \\
+ 2\nu \Delta t \|\mathbb{D}(\widehat{\boldsymbol{u}}_{ch}^{n+1})\|^{2} + \beta_{2} h \Delta t \left(\nabla (\boldsymbol{u}_{ch}^{n+1} - \boldsymbol{u}_{ch}^{n-1}), \nabla \widehat{\boldsymbol{u}}_{ch}^{n+1}\right) - \xi^{n+1} \Delta t \left(\boldsymbol{w}_{ch}^{n} \nabla \phi_{ch}^{n}, \widehat{\boldsymbol{u}}_{ch}^{n+1}\right) \\
+ \delta \Delta t \left(p_{ch}^{n+1} - p_{ch}^{n-1}, \widehat{p}_{ch}^{n+1}\right) + \Delta t \left(\nabla \cdot \boldsymbol{u}_{ch}^{n}, \widehat{p}_{ch}^{n+1}\right) - \Delta t \frac{\xi^{n+1}}{2} \left\langle \boldsymbol{u}_{ch}^{n} \cdot \boldsymbol{u}_{ch}^{n}, \widehat{\boldsymbol{u}}_{ch}^{n+1} \cdot \boldsymbol{n}_{c} \right\rangle \\
- \Delta t \left(p_{ch}^{n}, \nabla \cdot \widehat{\boldsymbol{u}}_{ch}^{n+1}\right) + \Delta t \xi^{n+1} \left\langle p_{mh}^{n}, \widehat{\boldsymbol{u}}_{ch}^{n+1} \cdot \boldsymbol{n}_{c} \right\rangle + \frac{\alpha \nu \sqrt{d}}{\sqrt{\text{trace}(\mathbf{II})}} \left\langle P_{\tau} \widehat{\boldsymbol{u}}_{ch}^{n+1}, P_{\tau} \widehat{\boldsymbol{u}}_{ch}^{n+1} \right\rangle = 0.$$

Then, we study the matrix part. Taking $q_h = \Delta t \hat{p}_{mh}^{n+1}$ in (3.16), $\boldsymbol{v}_h = \Delta t \hat{\boldsymbol{u}}_{mh}^{n+1}$ in (3.15) add these two equations to obtain

$$\Delta t \| \sqrt{\mathbb{K}^{-1}} \widehat{\boldsymbol{u}}_{mh}^{n+1} \|^{2} + \Delta t (\nabla \widehat{p}_{mh}^{n+1}, \widehat{\boldsymbol{u}}_{mh}^{n+1}) - \Delta t (\boldsymbol{w}_{mh}^{n} \nabla \phi_{mh}^{n}, \widehat{\boldsymbol{u}}_{mh}^{n+1}) - \Delta t (\widehat{\boldsymbol{u}}_{mh}^{n+1}, \nabla \widehat{p}_{mh}^{n+1})$$

$$+ \beta_{1} h \Delta t (\nabla (\boldsymbol{u}_{mh}^{n+1} - \boldsymbol{u}_{mh}^{n-1}), \nabla \widehat{\boldsymbol{u}}_{mh}^{n+1}) - \xi^{n+1} \Delta t \langle \boldsymbol{u}_{ch}^{n} \cdot \boldsymbol{n}_{c}, p_{mh}^{n+1} \rangle = 0.$$

$$(3.25)$$

Multiplying (3.19) by Δt , and adding (3.23), (3.24) and (3.25) together, we obtain

$$\frac{1}{2}[\|R^{n+1}\|^{2} - \|R^{n-1}\|^{2}]$$

$$= -\xi^{n+1} \Delta t \left[2\nu \|\mathbb{D}(\overline{\boldsymbol{u}}_{ch}^{n+1})\|^{2} + \|\sqrt{\mathbb{K}^{-1}}\overline{\boldsymbol{u}}_{mh}^{n+1}\|^{2} + M\|\nabla \overline{\boldsymbol{w}}_{h}^{n+1}\|^{2} + \frac{\alpha\nu\sqrt{d}}{\sqrt{\mathrm{trace}(\prod)}} \langle P_{\tau}\overline{\boldsymbol{u}}_{ch}^{n+1}, P_{\tau}\overline{\boldsymbol{u}}_{ch}^{n+1} \rangle \right]$$

$$+ \Delta t \xi^{n+1} S_{0} + \Delta t (1 - \xi^{n+1}) |S_{0}|.$$
(3.26)

It follows that

$$(R^{n+1})^2 \left[1 + \frac{\Delta t}{\overline{E}} (\mathcal{D}^{n+1} + |S_0| - S_0) \right] = (R^{n-1})^2 + 2\Delta t |S_0| > 0.$$

Hence the scheme is well-defined, and in particular $\xi^{n+1} > 0$. This completes the proof of Theorem 1. \square The modified energy law is stated in the following theorem.

Theorem 2 Under the assumption that source terms f(x), g(x) and h(x) are zero, the CNLF numerical scheme (3.12)-(3.19) is unconditionally stable with respect to the modified energy \mathcal{E}^{n+1} defined as

$$\mathcal{E}^{n+1} = \frac{1}{2}(|R^{n+1}|^2 + |R^n|^2), \tag{3.27}$$

in the sense of that

$$\mathcal{E}^{n+1} - \mathcal{E}^n = -\xi^{n+1} \Delta t \mathcal{D}^{n+1} \le 0, \tag{3.28}$$

where the energy dissipation \mathcal{D}^{n+1} is defined as in (3.22).

3.2 Decoupled energy-stable gPAV-BDF2 numerical scheme

Denoting

$$\tilde{v}^{n+1} = 2v^n - v^{n-1},\tag{3.29}$$

$$\xi^{n+1} = \frac{(R^{n+3/2})^2}{E(\overline{u}_{ch}^{n+3/2}, \overline{\phi}_h^{n+3/2})}.$$
(3.30)

By combining the second-order backward differentiation formula (BDF2) and the artificial compressible method, we develop the following gPAV-BDF2 method:

Step 1: Find $(\phi_h^{n+1}, w_h^{n+1}) \in Y_h \times Y_h$, such that for all $(\psi_h, \omega_h) \in Y_h \times Y_h$

$$\left(\frac{3\phi_h^{n+1} - 4\phi^n + \phi_h^{n-1}}{2\Delta t}, \psi_h\right) + \xi^{n+1}(\widetilde{\boldsymbol{u}}_h^{n+1} \cdot \nabla \widetilde{\phi}_h^{n+1}, \psi_h) + \left(M(\widetilde{\phi}_h^{n+1}) \nabla w_h^{n+1}, \nabla \psi_h = (h(\boldsymbol{x}), \psi_h), (3.31)\right)$$

$$(w_h^{n+1}, \omega_h) - \gamma \epsilon (\nabla \phi_h^{n+1}, \nabla \omega_h) - \xi^{n+1} \frac{\gamma}{\epsilon} (f(\widetilde{\phi}_h^{n+1}), \omega_h) - S(\phi_h^{n+1} - \widetilde{\phi}_h^{n+1}, \omega_h) = 0, \tag{3.32}$$

where

$$\widetilde{\boldsymbol{u}}_{h}^{n+1} := \begin{cases} 2\boldsymbol{u}_{ch}^{n} - \boldsymbol{u}_{ch}^{n-1}, & \boldsymbol{x} \in \Omega_{c}, \\ 2\boldsymbol{u}_{mh}^{n} - \boldsymbol{u}_{mh}^{n-1}, & \boldsymbol{x} \in \Omega_{m}. \end{cases}$$

$$(3.33)$$

Step 2: Find $(\boldsymbol{u}_{mh}^{n+1}, p_{mh}^{n+1}) \in \boldsymbol{X}_{mh} \times Q_{mh}$, such that for all $(\boldsymbol{v}_h, q_h) \in \boldsymbol{X}_{mh} \times Q_{mh}$

$$\mathbb{K}^{-1}(\boldsymbol{u}_{mh}^{n+1}, \boldsymbol{v}_h) + (\nabla p_{mh}^{n+1}, \boldsymbol{v}_h) - \xi^{n+1}(\widetilde{\boldsymbol{w}}_{mh}^{n+1} \nabla \widetilde{\boldsymbol{\phi}}_{mh}^{n+1}, \boldsymbol{v}_h) + \beta_1 h(\nabla (3\boldsymbol{u}_{mh}^{n+1} - 4\boldsymbol{u}_{mh}^n + \boldsymbol{u}_{ch}^{n-1}), \nabla \boldsymbol{v}_h) = 0,$$
(3.34)

$$-(\nabla \boldsymbol{u}_{mh}^{n+1}, \nabla q) - \xi^{n+1} \langle \widetilde{\boldsymbol{u}}_{ch}^{n+1} \cdot \boldsymbol{n}_c, q_h \rangle = (g(\boldsymbol{x}), q_h). \tag{3.35}$$

Step 3: Find $u_{ch}^{n+1} \in X_{ch}$, such that for all $v_h \in X_{ch}$

$$\left(\frac{3\boldsymbol{u}_{ch}^{n+1} - 4\boldsymbol{u}_{ch}^{n} + \boldsymbol{u}_{ch}^{n-1}}{2\Delta t}, \boldsymbol{v}_{h}\right) + \xi^{n+1}\left(\left(\widetilde{\boldsymbol{u}}_{ch}^{n+1} \cdot \nabla\right)\widetilde{\boldsymbol{u}}_{ch}^{n+1}, \boldsymbol{v}_{h}\right) + \frac{\xi^{n+1}}{2}\left(\left(\nabla \cdot \widetilde{\boldsymbol{u}}_{ch}^{n+1}\right)\widetilde{\boldsymbol{u}}_{ch}^{n+1}, \boldsymbol{v}\right) \\
+ 2\nu\left(\mathbb{D}(\boldsymbol{u}_{ch}^{n+1}), \mathbb{D}(\boldsymbol{v}_{h})\right) + \beta_{2}h\left(\nabla\left(3\boldsymbol{u}_{ch}^{n+1} - 4\boldsymbol{u}_{ch}^{n} + \boldsymbol{u}_{ch}^{n-1}\right), \nabla\boldsymbol{v}_{h}\right) - \xi^{n+1}\left(\widetilde{\boldsymbol{w}}_{ch}^{n+1} \nabla \widetilde{\boldsymbol{\phi}}_{ch}^{n+1}, \boldsymbol{v}_{h}\right) \\
- \frac{1}{3}\left(4p_{ch}^{n} - p_{ch}^{n-1}, \nabla \cdot \boldsymbol{v}_{h}\right) + \frac{1}{3\delta\Delta t}\left(\nabla \cdot \widetilde{\boldsymbol{u}}_{ch}^{n+1}, \nabla \cdot \boldsymbol{v}_{h}\right) - \frac{\xi^{n+1}}{2}\left\langle\widetilde{\boldsymbol{u}}_{ch}^{n+1} \cdot \widetilde{\boldsymbol{u}}_{ch}^{n+1}, \boldsymbol{v}_{h} \cdot \boldsymbol{n}_{c}\right\rangle \\
+ \xi^{n+1}\left\langle\widetilde{p}_{mh}^{n+1}, \boldsymbol{v}_{h} \cdot \boldsymbol{n}_{c}\right\rangle + \frac{\alpha\nu\sqrt{d}}{\sqrt{\text{trace}(\boldsymbol{\Pi})}}\left\langle P_{\tau}\boldsymbol{u}_{ch}^{n+1}, P_{\tau}\boldsymbol{v}_{h}\right\rangle = (f(\boldsymbol{x}), \boldsymbol{v}_{h}), \tag{3.36}$$

where β_2 is a positive parameter.

Step 4: Find $p_{ch}^{n+1} \in Q_{ch}$, such that for all $q_h \in Q_{ch}$

$$\delta \Delta t (3p_{ch}^{n+1} - 4p_{ch}^n + p_{ch}^{n-1}, q_h) + (\nabla \cdot \tilde{\boldsymbol{u}}_{ch}^{n+1}, q_h) = 0.$$
 (3.37)

Step 5: Find R^{n+1} , such that

$$\begin{split} \frac{(R^{n+3/2})^2 - (R^{n+1/2})^2}{\Delta t} &= (\frac{3\boldsymbol{u}_{ch}^{n+1} - 4\boldsymbol{u}_{ch}^n + \boldsymbol{u}_{ch}^{n-1}}{2\Delta t}, \boldsymbol{u}_{ch}^{n+1}) + \gamma \epsilon (\nabla \phi_h^{n+1}, \nabla \frac{3\phi_h^{n+1} - 4\phi_h^n + \phi_h^{n-1}}{2\Delta t}) \\ &+ 2\delta \Delta t^2 (\frac{3p_{ch}^{n+1} - 4p_{ch}^n + p_{ch}^{n-1}}{2\Delta t}, p_{ch}^{n+1}) + \xi^{n+1} \frac{\gamma}{\epsilon} (f(\widetilde{\phi}_h^{n+1}), \nabla \frac{3\phi_h^{n+1} - 4\phi_h^n + \phi_h^{n-1}}{2\Delta t}) \end{split}$$

$$+S(\phi_{h}^{n+1} - \tilde{\phi}_{h}^{n+1}, \frac{3\phi_{h}^{n+1} - 4\phi^{n} + \phi_{h}^{n-1}}{2})$$

$$+\beta_{1}h(\nabla(3u_{mh}^{n+1} - 4u_{mh}^{n} + u_{mh}^{n-1}), \nabla u_{mh}^{n+1}) + \beta_{2}h(\nabla(3u_{ch}^{n+1} - 4u_{ch}^{n} + u_{ch}^{n-1}), \nabla u_{ch}^{n+1})$$

$$+ \left[2\nu\|\mathbb{D}(u_{ch}^{n+1})\|^{2} - \frac{1}{3}(4p_{ch}^{n} - p_{ch}^{n-1}, \nabla \cdot u_{ch}^{n+1}) + \xi^{n+1}((\tilde{u}_{ch}^{n+1} \cdot \nabla)\tilde{u}_{ch}^{n+1}, u_{ch}^{n+1}) + M\|\nabla w_{h}^{n+1}\|^{2}$$

$$+ \frac{1}{3\delta\Delta t}(\nabla \cdot \tilde{u}_{ch}^{n+1}, \nabla \cdot u_{ch}^{n+1}) - \xi^{n+1}(\tilde{w}_{ch}^{n+1}\nabla\tilde{\phi}_{ch}^{n+1}, u_{ch}^{n+1}) + \frac{\xi^{n+1}}{2}((\nabla \cdot \tilde{u}_{ch}^{n+1})\tilde{u}_{ch}^{n+1}, u_{ch}^{n+1})$$

$$+(\nabla \cdot \tilde{u}_{ch}^{n+1}, p_{ch}^{n+1}) + (\nabla p_{mh}^{n+1}, u_{mh}^{n+1}) - \xi^{n+1}(\tilde{w}_{mh}^{n+1}\nabla\tilde{\phi}_{mh}^{n+1}, u_{mh}^{n+1}) - (u_{mh}^{n+1}, \nabla p_{mh}^{n+1})$$

$$+\mathbb{K}^{-1}\|u_{mh}^{n+1}\|^{2} + \xi^{n+1}(\tilde{u}_{h}^{n+1} \cdot \nabla\tilde{\phi}_{h}^{n+1}, w_{h}^{n+1}) - (f(x), u_{ch}^{n+1}) - (g(x), p_{mh}^{n+1}) - (h(x), w_{h}^{n+1})]$$

$$+\xi^{n+1}\langle\tilde{p}_{mh}^{n+1} - \frac{1}{2}|\tilde{u}_{ch}^{n+1}|^{2}, u_{ch}^{n+1} \cdot n_{c}\rangle - \xi^{n+1}\langle\tilde{u}_{ch}^{n+1} \cdot n_{c}, p_{mh}^{n+1}\rangle + \frac{\alpha\nu\sqrt{d}}{\sqrt{\text{trace}(\Pi)}}\langle P_{\tau}u_{ch}^{n+1}, P_{\tau}u_{ch}^{n+1}\rangle$$

$$+\xi^{n+1}\left[-2\nu\|\mathbb{D}(\breve{u}_{ch}^{n+1})\|^{2} - \mathbb{K}^{-1}\|\breve{u}_{mh}^{n+1}\|^{2} - M\|\nabla\breve{w}_{h}^{n+1}\|^{2} - \frac{\alpha\nu\sqrt{d}}{\sqrt{\text{trace}(\Pi)}}\langle P_{\tau}\breve{u}_{ch}^{n+1}, P_{\tau}\breve{u}_{ch}^{n+1}\rangle\right]$$

$$+\xi^{n+1}\tilde{S}_{0} + (1-\xi)|\breve{S}_{0}|, \tag{3.38}$$

where

$$\breve{S}_0 = (\mathbf{f}(\mathbf{x}), \breve{\mathbf{u}}_{ch}^{n+1}) + (g(\mathbf{x}), \breve{p}_{mh}^{n+1}) + (h(\mathbf{x}), \breve{\mathbf{w}}_h^{n+1}),$$
(3.39)

 $\overline{\pmb{u}}_{ch}^{n+3/2},\,\overline{\phi}_h^{n+3/2}$ are second order approximations of $\pmb{u}_{ch}^{n+1},\,\phi_h^{n+1},$ i.e.

$$\overline{v}^{n+3/2} = \frac{3}{2} \check{v}^{n+1} - \frac{1}{2} v^n, \quad v = \mathbf{u}_{ch}, \ \phi_h.$$

 $Remark\ 2$ Following the second order artificial compressible method, on can discretize (2.30)-(2.31) as

$$\frac{3\boldsymbol{u}_{ch}^{n+1} - 4\boldsymbol{u}_{ch}^{n} + \boldsymbol{u}_{ch}^{n-1}}{2\Delta t} + \xi^{n+1} \left(\widetilde{\boldsymbol{u}}_{ch}^{n+1} \cdot \nabla \right) \widetilde{\boldsymbol{u}}_{ch}^{n+1} + \frac{\xi^{n+1}}{2} \left(\nabla \cdot \widetilde{\boldsymbol{u}}_{ch}^{n+1} \right) \widetilde{\boldsymbol{u}}_{ch}^{n+1} + 2\nabla \cdot \left(\nu(\mathbb{D}(\boldsymbol{u}_{ch}^{n+1})) \right) \\
- \beta_{2}h\Delta (3\boldsymbol{u}_{ch}^{n+1} - 4\boldsymbol{u}_{ch}^{n} + \boldsymbol{u}_{ch}^{n-1}) - \xi^{n+1} \widetilde{\boldsymbol{w}}_{ch}^{n+1} \nabla \widetilde{\boldsymbol{\phi}}_{ch}^{n+1} + \nabla p_{ch}^{n+1} = f(\boldsymbol{x}), \tag{3.40}$$

$$\delta \Delta t (3p_{ch}^{n+1} - 4p_{ch}^{n} + p_{ch}^{n-1}) + \nabla \cdot \widetilde{\boldsymbol{u}}_{ch}^{n+1} = 0. \tag{3.41}$$

This system (3.40)-(3.41) seems to be a coupled system. However one can eliminate p_{ch}^{n+1} in (3.40) from (3.41) and derive

$$p_{ch}^{n+1} = \frac{1}{3} (4p_{ch}^n - p_{ch}^{n-1}) - \frac{1}{3\delta A t} \nabla \cdot \tilde{\boldsymbol{u}}_{ch}^{n+1}, \tag{3.42}$$

then plug (3.42) into (3.40) to obtain

$$\frac{3\boldsymbol{u}_{ch}^{n+1} - 4\boldsymbol{u}_{ch}^{n} + \boldsymbol{u}_{ch}^{n-1}}{2\Delta t} + \xi^{n+1} \left(\widetilde{\boldsymbol{u}}_{ch}^{n+1} \cdot \nabla \right) \widetilde{\boldsymbol{u}}_{ch}^{n+1} + \frac{\xi^{n+1}}{2} \left(\nabla \cdot \widetilde{\boldsymbol{u}}_{ch}^{n+1} \right) \widetilde{\boldsymbol{u}}_{ch}^{n+1} + 2\nabla \cdot \left(\nu(\mathbb{D}(\boldsymbol{u}_{ch}^{n+1})) \right) \\ + \frac{1}{3} \nabla (4p_{ch}^{n} - p_{ch}^{n-1}) - \frac{1}{3\delta \Delta t} \Delta \widetilde{\boldsymbol{u}}_{ch}^{n+1} - \beta_{2} h \Delta (3\boldsymbol{u}_{ch}^{n+1} - 4\boldsymbol{u}_{ch}^{n} + \boldsymbol{u}_{ch}^{n-1}) - \xi^{n+1} \widetilde{\boldsymbol{w}}_{ch}^{n+1} \nabla \widetilde{\boldsymbol{\phi}}_{ch}^{n+1} = f(\boldsymbol{x}).$$

Thereafter, by applying integration by parts and interface conditions, we obtain the full discretization (3.36) and (3.37). One can independently compute $\boldsymbol{u}_{ch}^{n+1}$ by solving (3.36) and p_{ch}^{n+1} by solving (3.37), that is the decoupling of velocity and pressure in Navier-Stokes equation.

We first prove the following property for the BDF2 numerical scheme (3.31)-(3.38).

Theorem 3 The approximation $(\boldsymbol{u}_{mh}^{n+1}, \boldsymbol{u}_{ch}^{n+1}, p_{ch}^{n+1}, \phi_h^{n+1})$ by the scheme (3.31)-(3.38) satisfies the following equality:

$$|R^{n+3/2}|^2 - |R^{n+1/2}|^2 = -\xi^{n+1} \Delta t \left[\check{\mathcal{D}}^{n+1} - \check{S}_0 \right] + \Delta t (1 - \xi^{n+1}) |\check{S}_0|, \tag{3.44}$$

where $\breve{\mathcal{D}}^{n+1}$ is given by

$$\check{\mathcal{D}}^{n+1} = 2\nu \|\mathbb{D}(\check{\mathbf{u}}_{ch}^{n+1})\|^2 + \|\sqrt{\mathbb{K}^{-1}}\check{\mathbf{u}}_{mh}^{n+1}\|^2 + \|\sqrt{M(\phi_h^n)}\nabla \check{\mathbf{w}}_h^{n+1}\|^2 + \frac{\alpha\nu\sqrt{d}}{\sqrt{trace(\prod)}} \langle P_{\tau}\check{\mathbf{u}}_{ch}^{n+1}, P_{\tau}\check{\mathbf{u}}_{ch}^{n+1} \rangle.$$
(3.45)

Therefore the scheme is well-defined with $\xi^{n+1} > 0$.

Proof. We first consider the Cahn-Hilliard equation on the whole domain Ω . Taking $\psi_h = \Delta t w_h^{n+1}$ and $\omega_h = -\frac{3\phi_h^{n+1} - 4\phi_h^n + \phi_h^{n-1}}{2}$ in (3.31) and (3.32), respectively, adding these resultants, we derive

$$\gamma \epsilon (\nabla \phi_h^{n+1}, \nabla \frac{\phi_h^{n+1} - \phi_h^{n-1}}{2}) + \xi^{n+1} \frac{\gamma}{\epsilon} (f(\widetilde{\phi}_h^{n+1}), \frac{3\phi_h^{n+1} - 4\phi_h^n + \phi_h^{n-1}}{2}) + \Delta t \xi^{n+1} (\widetilde{\boldsymbol{u}}_h^{n+1} \cdot \nabla \widetilde{\phi}_h^{n+1}, \boldsymbol{w}_h^{n+1}) \\ + \Delta t \| \sqrt{M(\widetilde{\phi}_h^{n+1})} \nabla \boldsymbol{w}_h^{n+1} \|^2 + S(\phi_h^{n+1} - \widetilde{\phi}_h^{n+1}, \frac{3\phi_h^{n+1} - 4\phi^n + \phi_h^{n-1}}{2}) = 0,$$
 (3.46)

Next, we consider the conduit part. Taking the test function $v_h = \Delta t u_{ch}^{n+1}$ in (3.36), and $q_h = p_{ch}^{n+1}$ in (3.37), respective, we take the sum to obtain

$$\left(\frac{3\boldsymbol{u}_{ch}^{n+1} - 4\boldsymbol{u}_{ch}^{n} + \boldsymbol{u}_{ch}^{n-1}}{2}, \boldsymbol{u}_{ch}^{n+1}\right) + \Delta t \boldsymbol{\xi}^{n+1} \left(\left(\widetilde{\boldsymbol{u}}_{ch}^{n+1} \cdot \nabla\right) \widetilde{\boldsymbol{u}}_{ch}^{n+1}, \boldsymbol{u}_{ch}^{n+1}\right) + \Delta t \frac{\boldsymbol{\xi}^{n+1}}{2} \left(\left(\nabla \cdot \widetilde{\boldsymbol{u}}_{ch}^{n+1}\right) \widetilde{\boldsymbol{u}}_{ch}^{n+1}, \boldsymbol{u}_{ch}^{n+1}\right) \\
+ 2\Delta t \nu \|\mathbb{D}(\boldsymbol{u}_{ch}^{n+1})\|^{2} + \Delta t \beta_{2} h \left(\nabla (3\boldsymbol{u}_{ch}^{n+1} - 4\boldsymbol{u}_{ch}^{n} + \boldsymbol{u}_{ch}^{n-1}), \nabla \boldsymbol{u}_{ch}^{n+1}\right) - \Delta t \boldsymbol{\xi}^{n+1} \left(\widetilde{\boldsymbol{w}}_{ch}^{n+1} \nabla \widetilde{\boldsymbol{\phi}}_{ch}^{n+1}, \boldsymbol{u}_{ch}^{n+1}\right) \\
- \frac{1}{3} \left(4p_{ch}^{n} - p_{ch}^{n-1}, \nabla \cdot \boldsymbol{u}_{ch}^{n+1}\right) + \frac{1}{3\delta\Delta t} \left(\nabla \cdot \widetilde{\boldsymbol{u}}_{ch}^{n+1}, \nabla \cdot \boldsymbol{u}_{ch}^{n+1}\right) + \delta\Delta t \left(3p_{ch}^{n+1} - 4p_{ch}^{n} + p_{ch}^{n-1}, p_{ch}^{n+1}\right) \\
+ \left(\nabla \cdot \widetilde{\boldsymbol{u}}_{ch}^{n+1}, p_{ch}^{n+1}\right) + \Delta t \boldsymbol{\xi}^{n+1} \left\langle \widetilde{p}_{mh}^{n+1}, \boldsymbol{u}_{ch}^{n+1} \cdot \boldsymbol{n}_{c} \right\rangle - \Delta t \frac{\boldsymbol{\xi}^{n+1}}{2} \left\langle \widetilde{\boldsymbol{u}}_{ch}^{n+1} \cdot \widetilde{\boldsymbol{u}}_{ch}^{n+1}, \boldsymbol{u}_{ch}^{n+1} \cdot \boldsymbol{n}_{c} \right\rangle \\
+ \Delta t \frac{\alpha \nu \sqrt{d}}{\sqrt{\text{trace}(\boldsymbol{H})}} \left\langle P_{\tau} \boldsymbol{u}_{ch}^{n+1}, P_{\tau} \boldsymbol{u}_{ch}^{n+1} \right\rangle = 0. \tag{3.47}$$

Then, we study the matrix part. Taking $q_h = \Delta t p_{mh}^{n+1}$ in (3.35), $\boldsymbol{v}_h = \Delta t \boldsymbol{u}_{mh}^{n+1}$ in (3.34)add these two equations to obtain

$$\begin{split} \Delta t \| \sqrt{\mathbb{K}^{-1}} \boldsymbol{u}_{mh}^{n+1} \|^2 + \Delta t (\nabla p_{mh}^{n+1}, \boldsymbol{u}_{mh}^{n+1}) - \Delta t (\widetilde{\boldsymbol{w}}_{mh}^{n+1} \nabla \widetilde{\boldsymbol{\phi}}_{mh}^{n+1}, \boldsymbol{u}_{mh}^{n+1}) - \Delta t (\boldsymbol{u}_{mh}^{n+1}, \nabla p_{mh}^{n+1}) \\ + \Delta t \beta_1 h (\nabla (3 \boldsymbol{u}_{mh}^{n+1} - 4 \boldsymbol{u}_{mh}^n + \boldsymbol{u}_{mh}^{n-1}), \nabla \boldsymbol{u}_{mh}^{n+1}) - \xi^{n+1} \Delta t (\widetilde{\boldsymbol{u}}_{ch}^{n+1} \cdot \boldsymbol{n}_c, p_{mh}^{n+1}) = 0. \ (3.48) \end{split}$$

Multiplying (3.38) by Δt , and adding (3.46), (3.47) and (3.48) together, we obtain

$$(R^{n+3/2})^2 - (R^{n+1/2})^2$$

$$= -\Delta t \xi^{n+1} \left[2\nu \| \mathbb{D}(\breve{\boldsymbol{u}}_{ch}^{n+1}) \|^{2} + \mathbb{K}^{-1} \| \breve{\boldsymbol{u}}_{mh}^{n+1} \|^{2} + M \| \nabla \breve{\boldsymbol{w}}_{h}^{n+1} \|^{2} + \frac{\alpha \nu \sqrt{d}}{\sqrt{\operatorname{trace}(\prod)}} \langle P_{\tau} \breve{\boldsymbol{u}}_{ch}^{n+1}, P_{\tau} \breve{\boldsymbol{u}}_{ch}^{n+1} \rangle \right]$$

$$+ \Delta t \breve{S}_{0} \xi^{n+1} + \Delta t (1 - \xi^{n+1}) |\breve{S}_{0}|.$$
(3.49)

This completes the proof of Theorem 3.

Theorem 4 Under the assumption that source terms f(x), g(x) and h(x) are zero, the BDF2 numerical scheme (3.31)-(3.38) is unconditionally stable with respect to the modified energy $\mathcal{E}^{n+3/2}$ defined as

$$\mathcal{E}^{n+3/2} = |R^{n+3/2}|^2,\tag{3.50}$$

on the sense of that

$$\mathcal{E}^{n+3/2} - \mathcal{E}^{n+1/2} = -\xi^{n+1} \Delta t \tilde{\mathcal{D}}^{n+1} \le 0, \tag{3.51}$$

where the energy dissipation $\tilde{\mathcal{D}}^{n+1}$ is defined as in (3.45).

Remark 3 Note that the above gPAV-CNLF and gPAV-BDF2 schemes are second-order accurate decoupled linear methods for the CHNSD system. In particular, $(\phi_h^{n+1}, w_h^{n+1})$, $(\boldsymbol{u}_{mh}^{n+1}, p_{mh}^{n+1})$, $\boldsymbol{u}_{ch}^{n+1}$, p_{ch}^{n+1} , and \mathbb{R}^{n+1} can be solved individually. More details on the implementation are discussed in Section 4. Therefore, one only needs to solve a sequence of small linear algebra systems, which renders very efficient computations in practice.

4 Implementation

We detail how to implement the gPAV-CNLF scheme (3.12)-(3.19) and the gPAV-BDF2 scheme (3.31)-(3.38) in a parallel decoupled manner. Since ξ is a scalar variable independent of spatial variable, we introduce the following splitting [68, 65]

$$\begin{aligned} w_h^{n+1} &= w_{1h}^{n+1} + \xi^{n+1} w_{2h}^{n+1}, & \phi_h^{n+1} &= \phi_{1h}^{n+1} + \xi^{n+1} \phi_{2h}^{n+1}, \\ p_{mh}^{n+1} &= p_{1mh}^{n+1} + \xi^{n+1} p_{2mh}^{n+1}, & p_{ch}^{n+1} &= p_{1ch}^{n+1} + \xi^{n+1} p_{2ch}^{n+1}, \\ \boldsymbol{u}_{mh}^{n+1} &= \boldsymbol{u}_{1mh}^{n+1} + \xi^{n+1} \boldsymbol{u}_{2mh}^{n+1}, & \boldsymbol{u}_{ch}^{n+1} &= \boldsymbol{u}_{1ch}^{n+1} + \xi^{n+1} \boldsymbol{u}_{2ch}^{n+1}. \end{aligned} \tag{4.1}$$

$$p_{mh}^{n+1} = p_{1mh}^{n+1} + \xi^{n+1} p_{2mh}^{n+1}, \quad p_{ch}^{n+1} = p_{1ch}^{n+1} + \xi^{n+1} p_{2ch}^{n+1}, \tag{4.2}$$

$$\boldsymbol{u}_{mh}^{n+1} = \boldsymbol{u}_{1mh}^{n+1} + \xi^{n+1} \boldsymbol{u}_{2mh}^{n+1}, \quad \boldsymbol{u}_{ch}^{n+1} = \boldsymbol{u}_{1ch}^{n+1} + \xi^{n+1} \boldsymbol{u}_{2ch}^{n+1}. \tag{4.3}$$

4.1 Implementation of the gPAV-CNLF numerical method

Denote

Then, we have

$$\overline{v}_h^{n+1} = \frac{1}{2}(v_{1h}^{n+1} + v_h^n) + \frac{1}{2}v_{2h}^{n+1}. \tag{4.5}$$

Replacing $(w_h^{n+1}, \phi_h^{n+1}, p_{mh}^{n+1}, p_{ch}^{n+1}, \boldsymbol{u}_{mh}^{n+1}, \boldsymbol{u}_{ch}^{n+1})$ in (3.12)-(3.19) by using (4.1), (4.2) and (4.3), we decompose the equations (3.12)-(3.19) according to ξ^{n+1} :

Step 1: Find $(\phi_{1h}^{n+1}, w_{1h}^{n+1}) \in Y_h \times Y_h$, such that

$$\left(\frac{\phi_{1h}^{n+1} - \phi_h^{n-1}}{2\Delta t}, \psi_h\right) + \left(M(\phi_h^n) \nabla \frac{w_{1h}^{n+1} + w_h^{n-1}}{2}, \nabla \psi_h\right) = 0, \ \forall \psi_h \in Y_h, \tag{4.6}$$

$$\left(\frac{w_{1h}^{n+1} + w_{h}^{n-1}}{2}, \omega_{h}\right) - \gamma \epsilon \left(\nabla \frac{\phi_{1h}^{n+1} + \phi_{h}^{n-1}}{2}, \nabla \omega_{h}\right) - S(\phi_{1h}^{n+1} - \phi_{h}^{n-1}, \omega_{h}) = 0, \ \forall \omega_{h} \in Y_{h}.$$
 (4.7)

Find $(\phi_{2h}^{n+1}, w_{2h}^{n+1}) \in Y_h \times Y_h$, such that

$$(\frac{\phi_{2h}^{n+1}}{2\Delta t}, \psi_h) + (\mathbf{u}_h^n \cdot \nabla \phi_h^n, \psi_h) + \frac{1}{2} (M(\phi_h^n) \nabla w_{2h}^{n+1}, \nabla \psi_h) = 0, \ \forall \psi_h \in Y_h,$$
(4.8)

$$\frac{1}{2}(w_{2h}^{n+1},\omega_h) - \frac{1}{2}\gamma\epsilon(\nabla\phi_{2h}^{n+1},\nabla\omega_h) - \frac{\gamma}{\epsilon}(f(\phi_h^n),\omega_h) - S(\phi_{2h}^{n+1},\omega_h) = 0, \ \forall \omega_h \in Y_h.$$
 (4.9)

Step 2: Find $(\boldsymbol{u}_{1mh}^{n+1}, p_{1mh}^{n+1}) \in \boldsymbol{X}_{mh} \times Q_{mh}$, such that

$$\mathbb{K}^{-1}(\boldsymbol{u}_{1mh}^{n+1}, \boldsymbol{v}_h) + (\nabla \frac{p_{1mh}^{n+1} + p_{mh}^{n-1}}{2}, \boldsymbol{v}_h) + \beta_1 h(\nabla (\boldsymbol{u}_{1mh}^{n+1} - \boldsymbol{u}_{mh}^{n-1}), \nabla \boldsymbol{v}_h) = 0, \ \forall \boldsymbol{v}_h \in \boldsymbol{X}_{mh}, \quad (4.10)$$

$$-(u_{1mh}^{n+1}, \nabla q) = (g(x), q_h), \ \forall q_h \in Q_{mh}. \tag{4.11}$$

Find $(\boldsymbol{u}_{2mh}^{n+1}, p_{2mh}^{n+1}) \in \boldsymbol{X}_{mh} \times Q_{mh}$, such that

$$\mathbb{K}^{-1}(\boldsymbol{u}_{2mh}^{n+1}, \boldsymbol{v}_h) + (\nabla p_{2mh}^{n+1}, \boldsymbol{v}_h) - (w_{mh}^n \nabla \phi_{mh}^n, \boldsymbol{v}_h) + \beta_1 h(\nabla \boldsymbol{u}_{2mh}^{n+1}, \nabla \boldsymbol{v}_h) = 0, \ \forall \, \boldsymbol{v}_h \in \boldsymbol{X}_{mh}, \quad (4.12)$$

$$-(\boldsymbol{u}_{2mh}^{n+1}, \nabla q) - \langle \boldsymbol{u}_{ch}^{n} \cdot \boldsymbol{n}_{c}, q_{h} \rangle = 0, \ \forall q_{h} \in Q_{mh}.$$

$$(4.13)$$

Step 3: Find $u_{1ch}^{n+1} \in X_{ch}$, such that

$$\left(\frac{\boldsymbol{u}_{1ch}^{n+1} - \boldsymbol{u}_{ch}^{n-1}}{2\Delta t}, \boldsymbol{v}_{h}\right) + \nu\left(\mathbb{D}(\boldsymbol{u}_{1ch}^{n+1} + \boldsymbol{u}_{ch}^{n-1}), \mathbb{D}(\boldsymbol{v}_{h})\right) - \left(p_{ch}^{n}, \nabla \cdot \boldsymbol{v}_{h}\right) + \beta_{2}h\left(\nabla(\boldsymbol{u}_{1ch}^{n+1} - \boldsymbol{u}_{ch}^{n-1}), \nabla \boldsymbol{v}_{h}\right) \\
+ \frac{\alpha\nu\sqrt{d}}{\sqrt{\operatorname{trace}(\boldsymbol{\Pi})}} \left\langle P_{\tau} \frac{\boldsymbol{u}_{1ch}^{n+1} + \boldsymbol{u}_{ch}^{n-1}}{2}, P_{\tau}\boldsymbol{v}_{h} \right\rangle = 0, \ \forall \, \boldsymbol{v}_{h} \in \boldsymbol{X}_{ch}. \tag{4.14}$$

Find $\boldsymbol{u}_{2ch}^{n+1} \in \boldsymbol{X}_{ch}$, such that

$$\left(\frac{\boldsymbol{u}_{2ch}^{n+1}}{2\Delta t}, \boldsymbol{v}_{h}\right) + \left(\left(\boldsymbol{u}_{ch}^{n} \cdot \nabla\right) \boldsymbol{u}_{ch}^{n}, \boldsymbol{v}_{h}\right) + \nu\left(\mathbb{D}(\boldsymbol{u}_{2ch}^{n+1}), \mathbb{D}(\boldsymbol{v}_{h})\right) - \left(\boldsymbol{w}_{ch}^{n} \nabla \phi_{ch}^{n}, \boldsymbol{v}_{h}\right) + \langle p_{mh}^{n}, \boldsymbol{v}_{h} \cdot \boldsymbol{n}_{c}\rangle
+ \frac{1}{2}\left(\left(\nabla \cdot \boldsymbol{u}_{ch}^{n}\right) \boldsymbol{u}_{ch}^{n}, \boldsymbol{v}_{h}\right) + \beta_{2}h\left(\nabla \boldsymbol{u}_{2ch}^{n+1}, \nabla \boldsymbol{v}_{h}\right) - \frac{1}{2}\langle \boldsymbol{u}_{ch}^{n} \cdot \boldsymbol{u}_{ch}^{n}, \boldsymbol{v}_{h} \cdot \boldsymbol{n}_{c}\rangle
+ \frac{\alpha\nu\sqrt{d}}{\sqrt{\operatorname{trace}(\boldsymbol{\Pi})}}\langle P_{\tau}\frac{\boldsymbol{u}_{2ch}^{n+1}}{2}, P_{\tau}\boldsymbol{v}_{h}\rangle = 0, \ \forall \boldsymbol{v}_{h} \in \boldsymbol{X}_{ch}.$$
(4.15)

Step 4: Find $p_{1ch}^{n+1} \in Q_{ch}$, such that

$$\delta \Delta t(p_{1ch}^{n+1} - p_{ch}^{n-1}, q_h) + (\nabla \cdot \boldsymbol{u}_{ch}^n, q) = 0, \ \forall \, q_h \in Q_{ch}. \tag{4.16}$$

Find $p_{2ch}^{n+1} \in Q_{ch}$, such that

$$\delta \Delta t(p_{2ch}^{n+1}, q_h) = 0, \ \forall q_h \in Q_{ch}. \tag{4.17}$$

Step 5: Find ξ^{n+1} , such that

$$\xi^{n+1} = \frac{|R^{n-1}|^2 + 2\Delta t S_0}{E(\overline{\boldsymbol{u}}_{ch}^{n+1}, \overline{\phi}_h^{n+1}) + 2\Delta t \mathcal{D}^{n+1} + 2\Delta t (|S_0| - S_0)},\tag{4.18}$$

which is derive from (3.26) by plugging (3.11). Once we have ξ^{n+1} , we update R^{n+1} by

$$R^{n+1} = \sqrt{\xi^{n+1} E(\overline{u}_{ch}^{n+1}, \overline{\phi}_h^{n+1})}, \tag{4.19}$$

where $\overline{\boldsymbol{u}}_{ch}^{n+1}$, $\overline{\phi}_h^{n+1}$ is defined in (4.5), \mathcal{D}^{n+1} is given in (3.22), S_0 is defined in (3.20), and

$$E(\overline{\boldsymbol{u}}_{ch}^{n+1}, \overline{\phi}_{h}^{n+1}) = \frac{1}{2} \|\overline{\boldsymbol{u}}_{ch}^{n+1}\|^{2} + \frac{\gamma\epsilon}{2} \|\nabla \overline{\phi}_{h}^{n+1}\|^{2} + \frac{1}{\epsilon} (F(\overline{\phi}_{h}^{n+1}), 1) + \delta \Delta t^{2} \|\overline{p}_{ch}^{n+1}\|^{2}.$$

Lemma 2 The scalar ξ^{n+1} in (4.18) and R^{n+1} in (4.19) are quaranteed to be positive at all time steps.

4.2 Implementation of the gPAV-BDF2 numerical method

Following the same splitting strategy we implement the BDF2 numerical scheme (3.31)-(3.38) as follows:

Step 1: Find $(\phi_{1h}^{n+1}, w_{1h}^{n+1}) \in Y_h \times Y_h$, such that

$$\left(\frac{3\phi_{1h}^{n+1} - 4\phi^n + \phi_h^{n-1}}{2\Delta t}, \psi_h\right) + \left(M(\widetilde{\phi}_h^{n+1})\nabla w_{1h}^{n+1}, \nabla \psi_h\right) = (h(\boldsymbol{x}), \psi_h), \ \forall \psi_h \in Y_h, \tag{4.20}$$

$$(w_{1h}^{n+1}, \omega_h) - \gamma \epsilon(\nabla \phi_{1h}^{n+1}, \nabla \omega_h) - S(3\phi_{1h}^{n+1} - 4\phi_h^n + \phi_h^{n-1}, \psi_h) = 0, \ \forall \omega_h \in Y_h.$$

$$(4.21)$$

Find $(\phi_{2h}^{n+1}, w_{2h}^{n+1}) \in Y_h \times Y_h$, such that

$$\left(\frac{3\phi_{2h}^{n+1}}{2\Delta t}, \psi_h\right) + \left(\widetilde{\boldsymbol{u}}_h^{n+1} \cdot \nabla \widetilde{\phi}_h^{n+1}, \psi_h\right) + \left(M(\widetilde{\phi}_h^{n+1}) \nabla w_{2h}^{n+1}, \nabla \psi_h\right) m = 0, \quad \forall \, \psi_h \in Y_h, \tag{4.22}$$

$$(w_{2h}^{n+1}, \omega_h) - \gamma \epsilon(\nabla \phi_{2h}^{n+1}, \nabla \omega_h) - \frac{\gamma}{\epsilon} (f(\widetilde{\phi}_h^{n+1}), \omega_h) - S(3\phi_{2h}^{n+1}, \psi_h) = 0, \ \forall \, \omega_h \in Y_h.$$
 (4.23)

Step 2: Find $(\boldsymbol{u}_{1mh}^{n+1}, p_{1mh}^{n+1}) \in \boldsymbol{X}_{mh} \times Q_{mh}$, such that

$$\mathbb{K}^{-1}(\boldsymbol{u}_{1mh}^{n+1}, \boldsymbol{v}_h) + (\nabla p_{1mh}^{n+1}, \boldsymbol{v}_h) + \beta_1 h(\nabla (3\boldsymbol{u}_{1mh}^{n+1} - 4\boldsymbol{u}_{mh}^n + \boldsymbol{u}_{mh}^{n-1}), \nabla \boldsymbol{v}_h) = 0, \ \forall \, \boldsymbol{v}_h \in \boldsymbol{X}_{mh}, \quad (4.24)$$

$$-(\nabla \boldsymbol{u}_{1mh}^{n+1}, \nabla q) = (g(\boldsymbol{x}), q_h), \ \forall q_h \in Q_{mh}. \tag{4.25}$$

Find $(\boldsymbol{u}_{2mh}^{n+1}, p_{2mh}^{n+1}) \in \boldsymbol{X}_{mh} \times Q_{mh}$, such that

$$\mathbb{K}^{-1}(\boldsymbol{u}_{2mh}^{n+1},\boldsymbol{v}_h) + \mathbb{K}(\nabla p_{2mh}^{n+1},\boldsymbol{v}_h) - \mathbb{K}(\widetilde{w}_{mh}^{n+1}\nabla\widetilde{\phi}_{mh}^{n+1},\boldsymbol{v}_h) + \beta_1 h(\nabla(3\boldsymbol{u}_{2mh}^{n+1}),\nabla\boldsymbol{v}_h) = 0, \ \forall \, \boldsymbol{v}_h \in \boldsymbol{X}_{mh},$$

$$(4.26)$$

$$-(\nabla \boldsymbol{u}_{2mh}^{n+1}, \nabla q) - \langle \widetilde{\boldsymbol{u}}_{ch}^{n+1} \cdot \boldsymbol{n}_c, q_h \rangle = 0, \ \forall \, q_h \in Q_{mh}. \tag{4.27}$$

Step 3: Find $u_{1ch}^{n+1} \in X_{ch}$, such that

$$\left(\frac{3\boldsymbol{u}_{1ch}^{n+1} - 4\boldsymbol{u}_{ch}^{n} + \boldsymbol{u}_{ch}^{n-1}}{2\Delta t}, \boldsymbol{v}_{h}\right) + 2\nu(\mathbb{D}(\boldsymbol{u}_{1ch}^{n+1}), \mathbb{D}(\boldsymbol{v}_{h})) + \beta_{2}h(\nabla(3\boldsymbol{u}_{1ch}^{n+1} - 4\boldsymbol{u}_{ch}^{n} + \boldsymbol{u}_{ch}^{n-1}), \nabla\boldsymbol{v}_{h}) \\
- \frac{1}{3}(4p_{ch}^{n} - p_{ch}^{n-1}, \nabla \cdot \boldsymbol{v}_{h}) + \frac{1}{3\delta\Delta t}(\nabla \cdot \widetilde{\boldsymbol{u}}_{ch}^{n+1}, \nabla \cdot \boldsymbol{v}_{h}) + \frac{\alpha\nu\sqrt{d}}{\sqrt{\text{trace}(\boldsymbol{\Pi})}}\langle P_{\tau}\boldsymbol{u}_{1ch}^{n+1}, P_{\tau}\boldsymbol{v}_{h}\rangle \\
= (f(\boldsymbol{x}), \boldsymbol{v}_{h}), \ \forall \boldsymbol{v}_{h} \in \boldsymbol{X}_{ch}. \tag{4.28}$$

Find $\boldsymbol{u}_{2ch}^{n+1} \in \boldsymbol{X}_{ch}$, such that

$$(\frac{3\boldsymbol{u}_{2ch}^{n+1}}{2\Delta t},\boldsymbol{v}_h) + \left(\left(\widetilde{\boldsymbol{u}}_{ch}^{n+1}\cdot\nabla\right)\widetilde{\boldsymbol{u}}_{ch}^{n+1},\boldsymbol{v}_h\right) + \frac{1}{2}\left(\left(\nabla\cdot\widetilde{\boldsymbol{u}}_{ch}^{n+1}\right)\widetilde{\boldsymbol{u}}_{ch}^{n+1},\boldsymbol{v}\right) + 2\nu(\mathbb{D}(\boldsymbol{u}_{2ch}^{n+1}),\mathbb{D}(\boldsymbol{v}_h)) \\ + \beta_2h(\nabla(3\boldsymbol{u}_{2ch}^{n+1}),\nabla\boldsymbol{v}_h) - \left(\widetilde{\boldsymbol{w}}_{ch}^{n+1}\nabla\widetilde{\boldsymbol{\phi}}_{ch}^{n+1},\boldsymbol{v}_h\right) + \left\langle\widetilde{\boldsymbol{p}}_{mh}^{n+1},\boldsymbol{v}_h\cdot\boldsymbol{n}_c\right\rangle - \frac{1}{2}\left\langle\widetilde{\boldsymbol{u}}_{ch}^{n+1}\cdot\widetilde{\boldsymbol{u}}_{ch}^{n+1},\boldsymbol{v}_h\cdot\boldsymbol{n}_c\right\rangle$$

$$+\frac{\alpha\nu\sqrt{d}}{\sqrt{\operatorname{trace}(\Pi)}}\langle P_{\tau}\boldsymbol{u}_{2ch}^{n+1}, P_{\tau}\boldsymbol{v}_{h}\rangle = (f(\boldsymbol{x}), \boldsymbol{v}_{h}), \ \forall \, \boldsymbol{v}_{h} \in \boldsymbol{X}_{ch}.$$

$$(4.29)$$

Step 4: Find $p_{1ch}^{n+1} \in Q_{ch}$, such that

$$\delta \Delta t (3p_{1ch}^{n+1} - 4p_{ch}^n + p_{ch}^{n-1}, q_h) + (\nabla \cdot \widetilde{\boldsymbol{u}}_{ch}^{n+1}, q_h) = 0, \ \forall \ q_h \in Q_{ch}.$$

$$(4.30)$$

Find $p_{2ch}^{n+1} \in Q_{ch}$, such that

$$\delta \Delta t(3p_{2ch}^{n+1}, q_h) = 0, \ \forall q_h \in Q_{ch}. \tag{4.31}$$

Step 5: Find ξ^{n+1} , such that

$$\xi^{n+1} = \frac{|R^{n+1/2}|^2 + \Delta t \breve{S}_0}{E(\overline{\boldsymbol{u}}_{ch}^{n+3/2}, \overline{\phi}_h^{n+3/2}) + \Delta t \breve{\mathcal{D}}^{n+1} + \Delta t (|\breve{S}_0| - \breve{S}_0)},\tag{4.32}$$

which is derived from (3.49) by plugging (3.30). Once we have ξ^{n+1} , we update $R^{n+3/2}$ by

$$R^{n+3/2} = \sqrt{\xi^{n+1} E(\overline{\boldsymbol{u}}_{ch}^{n+3/2}, \overline{\phi}_h^{n+3/2})}.$$
 (4.33)

Afterwards, R^{n+1} is updated by

$$R^{n+1} = \frac{2}{3}R^{n+3/2} + \frac{1}{3}R^n. (4.34)$$

Lemma 3 The scalar ξ^{n+1} in (4.32) and R^{n+1} in (4.34) are guaranteed to be positive positive at all time steps if the approximation $R^{n+1/2} > 0$.

In summary the second order gPAV-CNLF and gPAV-BDF2 schemes can be implemented as follows:

Algorithm 1 Implementation of gPAV-CNLF numerical method

```
1: Solve (\phi_{1h}^{n+1}, w_{1h}^{n+1}) from (4.6) and (4.7), independently; Solve (\phi_{2h}^{n+1}, w_{2h}^{n+1}) from (4.8) and (4.9), independently.
```

```
2: Solve (\boldsymbol{u}_{1mh}^{n+1}, p_{1mh}^{n+1}) from (4.10)-(4.11), (\boldsymbol{u}_{2mh}^{n+1}, p_{2mh}^{n+1}) from (4.12)-(4.13).
```

```
3: Solve \boldsymbol{u}_{1ch}^{n+1} from (4.14), \boldsymbol{u}_{2ch}^{n+1} from (4.15);
Solve p_{1ch}^{n+1} from (4.16), p_{2ch}^{n+1} from (4.17).
```

4: Solve ξ^{n+1} from (4.18).

```
5: Update w_h^{n+1} and \phi_h^{n+1} from (4.1);

Update p_{mh}^{n+1} and p_{ch}^{n+1} from (4.2);

Update u_{ch}^{n+1} and u_{mh}^{n+1} from (4.3);

Update R^{n+1} from (4.19).
```

5 Numerical examples

We first provide two examples to verify the convergence and energy dissipation as proved in Theorem 2 and Theorem 4. Then, we perform the simulation of square drop under non-diagonal hydraulic conductivity tensor with small eigenvalues. Finally, we simulate Saffman-Taylor instability, the dynamics of droplet in filter problem, and rising bubble with different densities to illustrate the compatibility and robustness of the gPAV schemes.

For Cahn-Hilliard equation in mixed formulation, we consider the linear finite elements. For Darcy equation and Navier-Stokes equation, we exploit the celebrated Taylor-Hood elements. That is, for $\phi - w - u_m - p_m - u_c - p_c$, we consider the $P_1 - P_1 - P_2 - P_1 - P_2 - P_1$ elements. The stabilized parameters are $\beta_1 = \beta_2 = 0.5$, S = 1 and $\delta = 0.71$ in the following numerical tests.

Algorithm 2 Implementation of gPAV-BDF2 numerical method

```
1: Solve (\phi_{1h}^{n+1}, w_{1h}^{n+1}) from (4.20) and (4.21), independently; Solve (\phi_{2h}^{n+1}, w_{2h}^{n+1}) from (4.22) and (4.23), independently.

2: Solve (u_{1mh}^{n+1}, p_{1mh}^{n+1}) from (4.24)-(4.25), (u_{2mh}^{n+1}, p_{2mh}^{n+1}) from (4.26)-(4.27).

3: Solve u_{1ch}^{n+1} from (4.28), u_{2ch}^{n+1} from (4.29).

4: Solve p_{1ch}^{n+1} from (4.30), p_{2ch}^{n+1} from (4.31).

5: Solve \xi^{n+1} from (4.32).

6: Solve R^{n+3/2} from (4.33); Update w_h^{n+1} and \phi_h^{n+1} from (4.1); Update p_{mh}^{n+1} and p_{ch}^{n+1} from (4.2); Update u_{ch}^{n+1} and u_{mh}^{n+1} from (4.3).

7: Update R^{n+1} from (4.34).
```

5.1 Accuracy and stability

Example 1: Convergence and accuracy. Consider the CHNSD model problem on $\Omega = [0, 1] \times [0, 2]$ where porous region $\Omega_m = [0, 1] \times [0, 1]$ and free flow region $\Omega_c = [0, 1] \times [1, 2]$. Set $M_m = 1$, $\gamma = 1$, $\epsilon = 1$, $\nu = 1$, $M_c = 1$ and $\mathbb{K} = \mathbb{I}$. The exact solutions are chosen as follows

$$\begin{cases}
\phi = g(x)g(y)\cos(\pi t), \\
p_m = g(x)g_m(y)\cos(\pi t), \\
\mathbf{u}_m = \mathbf{u}_c = [x^2(y-1)^2, -\frac{2}{3}x(y-1)^3]^T\cos(\pi t), \\
p_c = g(x)g_c(y)\cos(\pi t),
\end{cases} (5.1)$$

where $g(x) = x^2(x-1)^2$, $g_m(y) = y^2(y-1)^2$, $g_c(y) = (y-1)^2(y-2)^2$. The boundary conditions and source terms are given with respect to exact solution. Denote the numerical errors in L^2 - norm as as $\|e\|_v = \|v_h^n - v(t_n)\|$ between numerical solution v_h^n and exact solution $v(t_n)$ as $\|e\|_v = \|v_h^n - v(t_n)\|$, where $v = \mathbf{u}_c$, \mathbf{u}_m , p_m , ϕ . The numerical test is carried out up to terminal time T = 0.5. In order to verify the temporal convergence of proposed fully decoupled numerical method, we take mesh size $h = \frac{1}{2^k}$, k = 4, 5, 6, 7 and time step size $\Delta t = h$. The numerical errors and convergence order listed in Tables 1 and 2 suggest that the fully decoupled gPAV-CNLF and gPAV-BDF2 method can achieve the expected second order accuracy in time for variables \mathbf{u}_c , \mathbf{u}_m , p_m and ϕ .

In order to further illustrate the accuracy of our proposed gPAV method, we compare the numerical errors with those by the decoupled numerical method in [25] and auxiliary variable approaches developed in [26], respectively. From Table 3, it is observed that the accuracy of gPAV-CN and gPAV-BDF2 methods are comparable to that of numerical methods in [25] and [26] at larger mesh sizes, the numerical errors are smaller than those by other methods at very small mesh size $h = \frac{1}{256}$. The advantage of gPAV method becomes more obvious as the mesh size decreases. This is because that the gPAV-CN and gPAV-BDF2 methods are second order in time convergent while the designed numerical methods in [25] and [26] only have first order convergence rate in time.

1/h	$\ e_{\phi}\ $	order	$\ e_{oldsymbol{u}_c}\ $	order	$\ e_{p_c}\ $	order	$\ e_{\boldsymbol{u}_m}\ $	order	$\ e_{p_m}\ $	order
16	7.6634E-5		5.1473E-5		7.9111E-3		1.5940E-2		2.1904E-3	
32	1.0054E-5	2.93	1.2085E-5	2.10	1.7785E-3	2.15	4.8954E-3	1.70	5.2490E-4	2.06
64	1.3590E-6	2.89	2.2318E-6	2.44	2.6615E-4	2.72	1.3717E-3	1.84	1.0749E-4	2.29
128	1.8138E-7	2.91	$5.3820\mathrm{E}\text{-}7$	2.05	6.8983E-5	1.95	3.8496E-4	1.83	2.4783E-5	2.12

Table 1: The order of convergence for error norms of gPAV-CNLF algorithm with $\Delta t = h$.

Example 2: Energy stability. In this test, we verify the energy stability of proposed gPAV-CNLF and gPAV-BDF2 numerical methods by setting initial condition

$$\phi_0 = 0.24\cos(\pi x)\cos(2\pi y) + 0.4\cos(\pi x)\cos(3\pi y) \tag{5.2}$$

1/h	$\ e_{\phi}\ $	order $\ e_{\boldsymbol{u}_c}\ $	order $ e_{p_c} $	order $ e_{\boldsymbol{u}_m} $	order $ e_{p_m} $	order
16	2.6432E-4	4.1860E-5	1.3569E-3	1.6985E-2	7.4529E-3	
32	8.5919E-5	1.62 1.0862E-5	1.95 5.6540 E-4	1.26 5.1160E-3	1.73 2.2797E-3	1.71
64	2.3391E-5	1.88 2.7394E-6	1.99 1.1737E-4	2.27 1.3981E-3	1.87 5.5529E-4	2.04
128	6.0395 E-6	1.95 6.8686E-7	2.00 2.8694E-5	2.03 3.6713E-4	1.93 1.1786E-4	2.24

Table 2: The order of convergence for error norms of gPAV-BDF2 algorithm with $\Delta t = h$.

1/h		$\ e$	$ \phi $		$\ e_{oldsymbol{u}_c}\ $				
-/	gPAV-	gPAV-	[25]	[26]	gPAV-	gPAV-	[25]	[26]	
	CNLF	BDF2			CNLF	BDF2			
32	1.0054E-5	8.5919E-5	2.0585E-5	8.0230E-6	1.2085E-5	1.0862E-5	4.2737E-5	1.5856E-5	
64	1.3590 E-6	2.3391E-5	1.1229E-5	4.0561E-6	2.2318E-6	2.7394E-6	1.6519E-5	6.5148E-6	
128	1.8138E-7	6.0395E-6	5.7588E-6	2.0407E-6	5.3820E-7	6.8686E-7	6.1731E-6	2.9690E-6	
256	2.3637E-8	1.5353E-6	2.9583E-6	1.0203E-6	1.3086E-7	1.7196E-7	2.2290E-6	1.4341E-6	

Table 3: Numerical error norms of different numerical schemes with $\Delta t = h$.

on the computational domain $\Omega = [0,1] \times [0,2]$ with $\Omega_m = [0,1] \times [0,1]$ and $\Omega_c = [0,1] \times [1,2]$. Taking parameters M = 0.01, $\gamma = 0.01$, $\epsilon = 0.02$, $\nu = 1$, and $\mathbb{K} = 0.1\mathbb{I}$, we set the initial velocity, pressure and chemical potential to zero.

Figure 2 show the evolution of discrete energy $\mathcal{E} = (R(t))^2$ and true energy $E(\phi)$ of gPAV-CNLF and gPAV-BDF2 numerical methods with $\Delta t = 0.001$. From Figure 2, we can clearly observe that both $(R(t))^2$ and $E(\phi)$ decrease monotonically with time for both gPAV-CNLF and gPAV-BDF2 numerical methods, which agrees well with the theoretical results proven in Theorem 2 and Theorem 4. The histories curve of $(R(t))^2$ and $E(\phi)$ overlap with each other for both gPAV-CNLF and gPAV-BDF2 algorithms, which indicates the accuracy of our developed numerical schemes.

We discuss the influence of artificial viscosity parameters β_1 and β_2 for time step condition for convergence. Taking same parameters expect $\nu=0.01$, we plot the evolution of discrete energy $(R(t))^2$, true energy $E(\phi)$ and $\xi=\frac{(R(t))^2}{E(\phi)}$ in Figure 3 for both $\beta_1=\beta_2=0.5$ and $\beta_1=\beta_2=0$. When $\Delta t=0.001$, we observe that the time histories of $(R(t))^2$ and $E(\phi)$ are in well agreement with each other for both with and without stabilized parameters. For $\beta_1=\beta_2=0$ in Figure 3(a), the gPAV-BDF2 numerical methods gives accuracy results corresponding to $\Delta t=0.001$, it does not work with $\Delta t=0.01$ (the simulation will blow up); whereas a simulation by gPAV-BDF2 with non-zero stabilized parameters is stable and accurate under $\Delta t=0.01$ since the $(R(t))^2$ and $E(\phi)$ obtained with $\Delta t=0.01$ agree with quit well (with slight difference) as shown in Figures 3(b) and 3(c), thus, large $\Delta t=0.01$ is enough good for stable simulation. This demonstrates the effectiveness of relaxing the time step condition for convergence by the artificial viscosity stabilization technique.

In order to improve the accuracy and efficiency of proposed gPAV method, we perform the adaptive mesh strategy with the fundamental uniform mesh $h=\frac{1}{64}$ in the following experiments. The numerical results are similar for gPAV-CNLF and gPAV-BDF2 method, so we only present the numerical results of gPAV-BDF2 algorithm for the presentation compact in the following numerical tests.

Example 3: shape relaxation. In this test, we simulate the evolution of a square shaped circle drop under surface tension [25, 23], and consider more realistic case of hydraulic conductivity tensor with small eigenvalues. The hydraulic conductivity tensor is constructed as follows

$$\mathbb{K}(x,y) = \begin{pmatrix} k_{11}(x,y) & k_{12}(x,y) \\ k_{21}(x,y) & k_{22}(x,y) \end{pmatrix}$$

where $k_{11} = k_{22} \neq 0$ and $k_{12} = k_{21} \neq 0$, i.e. $\mathbb{K}(x, y)$ is non-diagonal but symmetric and positive definite. We take the initial condition as follows

$$\phi_0 = -\tanh\left((0.15 - \sqrt{(x - 0.3)^2 + (y - 0.5)^2})/(\sqrt{2}\epsilon)\right),$$

in domain $\Omega = [0,1] \times [0,2]$, $\Omega_c = [0,1] \times [1,2]$ and $\Omega_m = [0,1] \times [0,2]$ represent the upper and lower half of the square, respectively.

Choosing parameters M=0.1, $\gamma=0.01$, $\epsilon=0.01$, $k_{11}=k_{22}=10^{-3}$, $k_{12}=k_{21}=10^{-4}$, and time step size $\Delta t=0.001$, the morphological patterns of phase function ϕ is plotted in Figure 4 with

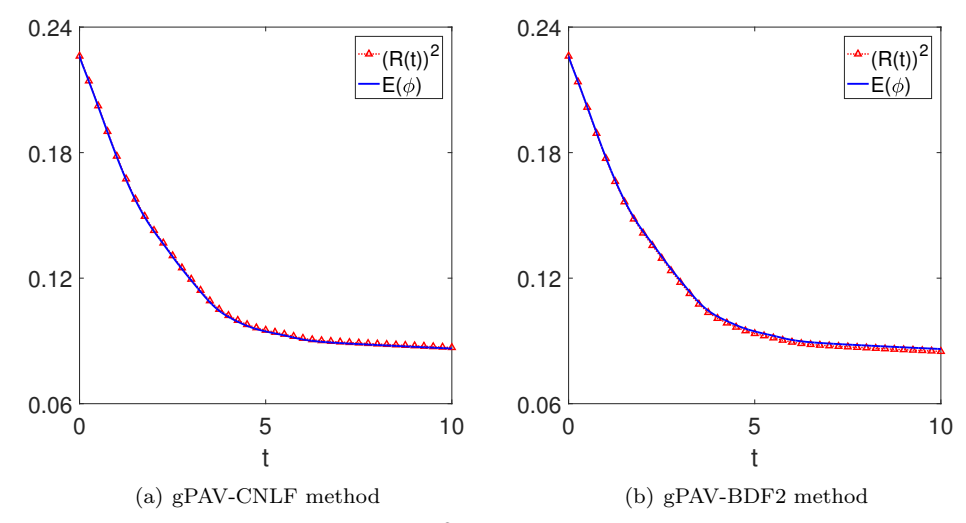


Fig. 2: Evolution of discrete energy $(R(t))^2$ and true energy $E(\phi)$ for gPAV numerical schemes.

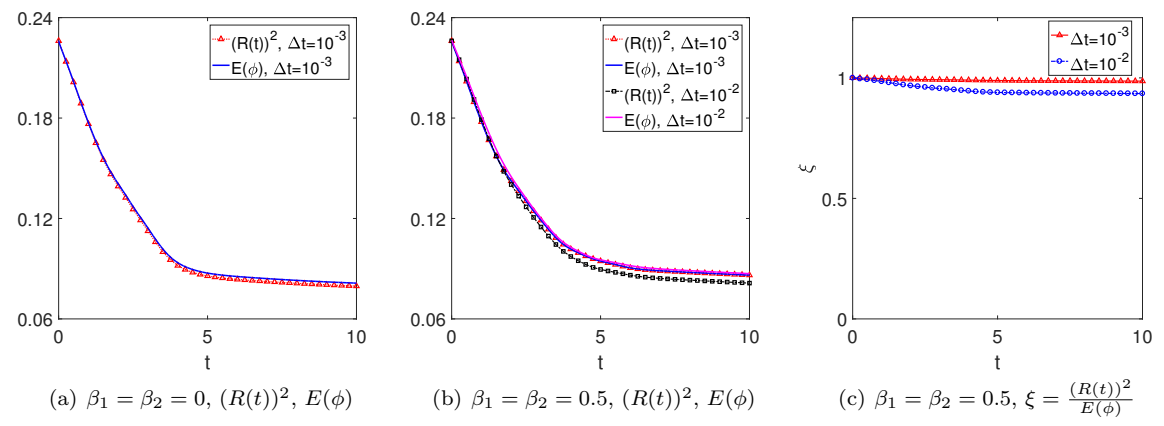


Fig. 3: Evolution of discrete energy $(R(t))^2$, true energy $E(\phi)$ and $\xi = \frac{(R(t))^2}{E(\phi)}$.

 $\nu=0.1,\ \nu=0.01$ and $\nu=0.001$, in which the red color and blue color respectively indicate $\phi=1$ and $\phi=-1$, the green line represents the interface $\Gamma=[0,1]\times\{y=1\}$ between free fluid region and porous media region. As shown in Figure 4, the square droplet gradually deforms into a stable equilibrium state corresponding to a circle shape under the influence of surface tension for both cases of $\nu=0.1,\ \nu=0.01$ and $\nu=0.001$.

By Comparing Figures 4(a), 4(b) and 4(c), we can see that as the viscosity decreases, the droplet deforms more rapidly in the free flow region, resulting in a more conspicuous asymmetry of the droplet shape on whole domain. This phenomenon shows that the relaxation in the free flow region is faster than that of the porous media region because the free flow velocity increases with decreasing viscosity. The relative discrete energy R^n/R^0 and relative mass $\int_{\Omega} \phi^n dx/\int_{\Omega} \phi^0 dx$ of numerical results are plotted in Figure 5. It reflects that the discrete mass is conserved and the discrete energy-decay property is satisfied.

5.2 Application

Example 4: Viscous finger. Saffman-Taylor fingering pattern instability [54, 17, 8] is a manifestation of a finger-shaped interface between displaced and displacing fluids that occurs in typical miscible displacement projects for oil recovery. The viscous fingering phenomenon occurs when a viscous fluid is displaced by another low-mobile fluid in the Hele-Shaw cell, which is of great significance to enhance

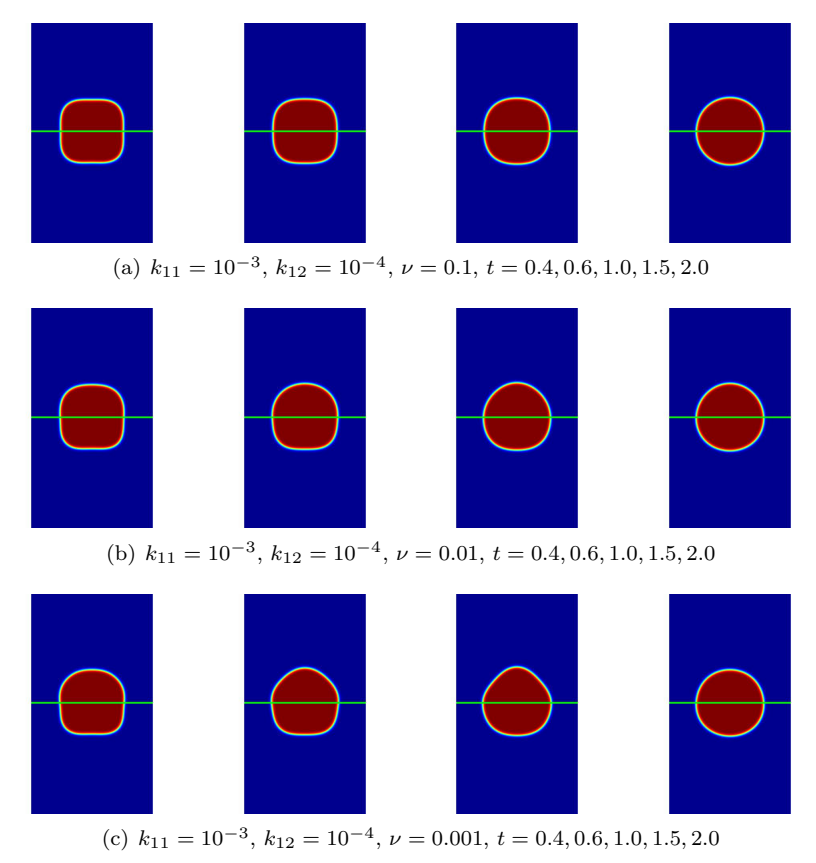


Fig. 4: Snapshots of phase variable for square drop with respect to different ν .

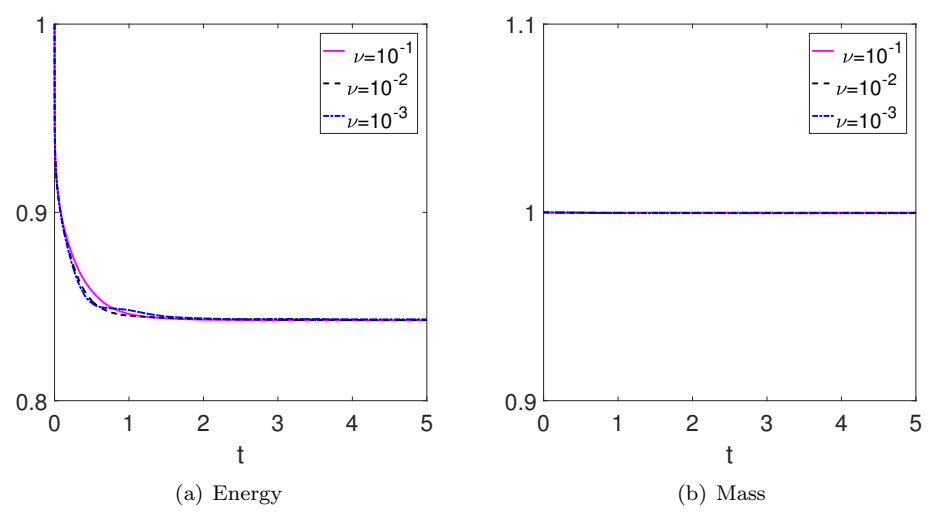


Fig. 5: Evolution of relative discrete energy and mass conservation of square shape.

oil recovery. In this test, we undertake to simulate the viscous fingering pattern, and further discuss the effects of the different viscous ratios upon viscous finger length and growth.

Parameters are taken as $\epsilon = 0.01$, $\gamma = 5 \times 10^{-4}$, M = 0.1 and $\nu(\phi_j) = \frac{\nu_1 - \nu_2}{2} \phi_j + \frac{\nu_1 + \nu_2}{2}$, j = 1, 2 corresponding to different viscosity ν_1 and ν_2 on a computational channel domain $\Omega = \Omega_c \bigcup \Omega_m$, $\Omega_c = [0, 0.5] \times [0, 1]$ and $\Omega_m = [0, 0.5] \times [1, 2]$. The initial configuration of the order parameter is given as follows

$$\phi_0(x,y) = -\tanh\left(\frac{4}{3\epsilon}\left(y - 0.8 + \frac{\cos(16\pi x)}{100}\right)\right). \tag{5.3}$$

The viscous fluid enters the free flow channel with a plug flow velocity of $u_{in} = 50$ on $\Gamma_{in} = [0, 0.5] \times \{0\}$ (bottom boundary).

Figure 6 exhibits the appearance and growth of finger pattern for different viscous ratios. Compared Figures 6(a) and 6(b) (or Figures 6(c) and 6(d)), we can find that the bigger viscous ratio, the longer the fingers. The expected numerical phenomena are well consistent with the numerical results reported in [19, 33]

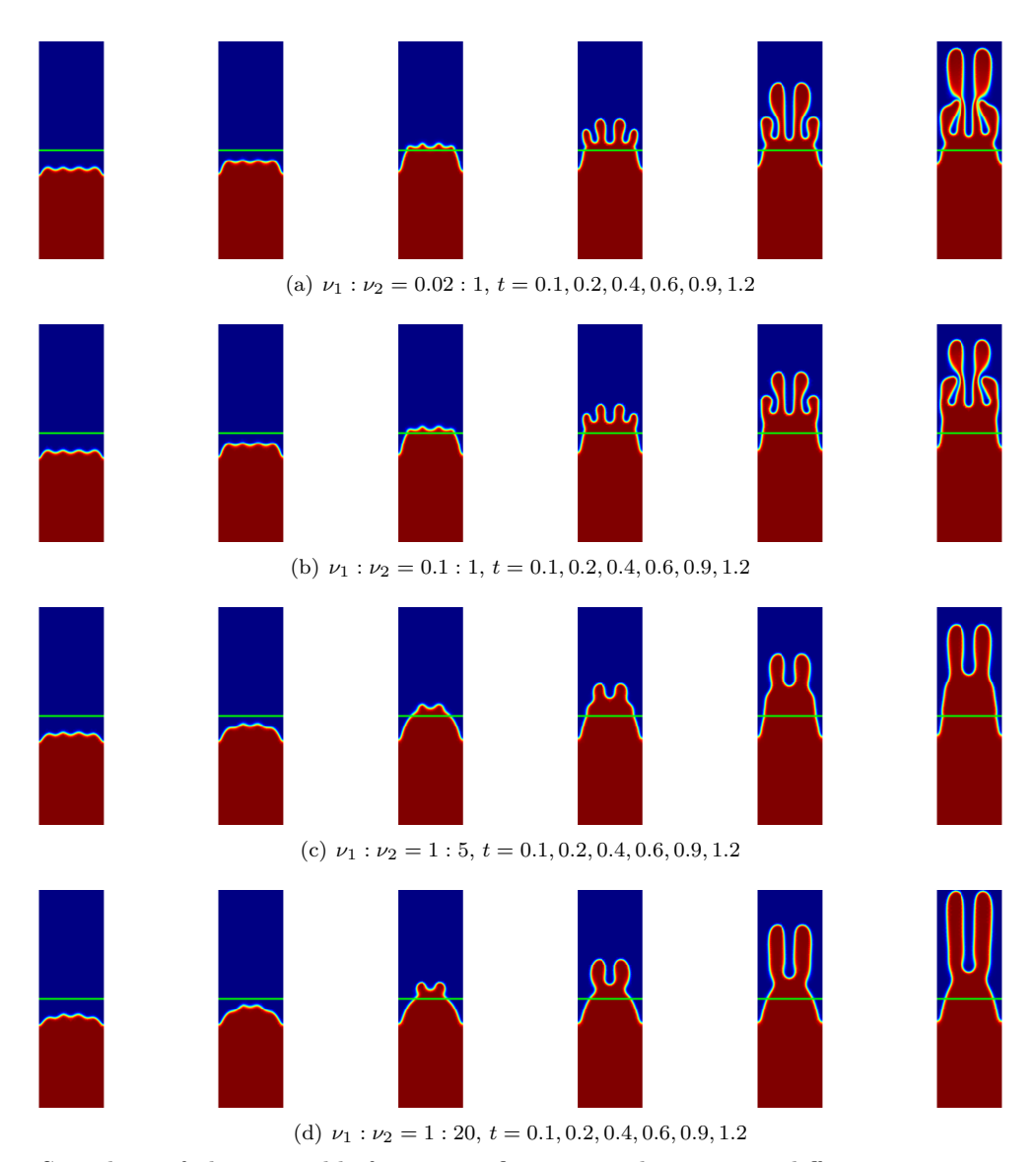


Fig. 6: Snapshots of phase variable for viscous fingering with respect to different viscosity ratios.

Example 5: Boundary-driven flow in filter problem.

In this test, we interest in the application to simulating realistic problem found in industrial filtration system [13, 36]. The coupled system consists of the fluid channel flow intercepted by a porous domain in Figures 7(a) and 7(c).

The computational domain is $\Omega = [0,3] \times [0,1]$ plotted in Figure 7, $\Omega = \Omega_c \cup \Omega_m$, $\Omega_c = \Omega_{1c} \cup \Omega_{2c}$, $\Omega_{1c} = [0,1] \times [0,1]$. The interface between free flow region and porous media is $\Gamma := \Gamma_1 \cup \Gamma_2$, where $\Gamma_1 = \{1\} \times [0,1]$ between Ω_{1c} and Ω_m , Γ_2 between Ω_m and Ω_{2c} . Two different types of interfaces are simulated, more specifically, straight interface $\Gamma_2 = \{2\} \times [0,1]$ as depicted in Figure 7(a), curve line $\Gamma_2 = \{(x,y)|x = \frac{3}{20}\sin(\pi y)\cos(\pi y) + 2, (x,y) \in \Omega\}$ as shown in Figure 7(c).

Choosing M=0.1, $\gamma=0.001$, $\epsilon=0.01$, and $\nu=0.1$, the initial pressure and chemical are zeros, and the initial configuration is defined as follows

$$\phi_0 = -\tanh\left((0.15 - \sqrt{(x - 0.3)^2 + (y - 0.5)^2}) / (\sqrt{2}\epsilon)\right),\tag{5.4}$$

which is shown in Figures 7(b) and 7(d) for two cases of domain (i.e. Figure 7(a) and Figure 7(c)), respectively. The parabolic inlet velocity $\mathbf{u}_c = -4y(y-1)$ is imposed on the left boundary $\Gamma_{in} := \{0\} \times [0,1]$.

Two types of computational domain are chosen as the free flow region and porous matrix region coupled with interfaces: two interfaces are both straight in Figure 7(a), one of the two interfaces is a straight line and the other is a curve in Figure 7(c). We extend numerical simulations that study uniform permeability fields (e.g. Example 4) to a more complicated problem with heterogeneous, isotropic permeability fields as plotted in Figure 8, including single crack permeability in Figure 8(a), trapezoid channel permeability in Figure 8(b), where the warmer color indicates higher hydraulic conductivity. The following three cases are simulated:

- Case I: computational domain is shown in Figure 7(a), meanwhile a porous medium has a single crack permeability field (i.e. Figure 8(a));
- Case II: computational domain is shown in Figure 7(a), meanwhile a porous medium has a trapezoid channel permeability field (i.e. Figure 8(b));
- Case III: computational domain is shown in Figure 7(c), meanwhile a porous medium has a trapezoid channel permeability field (i.e. Figure 8(b)).

Figure 9 displays the morphological evolution of phase profile ϕ from free flow region across the matrix, finally entering the free flow region through interfaces for three cases, more precisely, Figure 9(a) for Case I, Figure 9(b) for Case II, Figure 9(c) for Case III, respectively. From Figure 9, we can clearly see that the mobile moves toward the center region with high hydraulic conductivity at time t=0.5 and t=0.6, and deforms into a flat shape at the front propagating in porous media. It is evident that the mobile can seek pathways towards high permeability across the interface x=1 as expected due to the effect of hydraulic conductivity in porous media domain. As graphed in Figures 9(a) and 9(b), the contour of phase variable are distinct for heterogeneous mediums with single crack and trapezoid channel permeability. Therefore, the distribution of permeability fields has a significant influence on the development of phase patterns in the three coupled domains. The behaviour of the evolution is in good agreement with similar phenomena in [25, 47] illustrating the effectiveness of the proposed numerical methods. By comparing Figures 9(b) and 9(c), it is noticed that the appearance of droplet has obviously deformed under the influence of interface as desired, such as the dynamical diagram at t=1 and t=1.2. The reasonable numerical phenomena suggest the vital importance of the interface structure in multi-domain coupling problems [1, 59].

The speed and streamlines of velocity field in two type of domains with non-uniform matrix are graphed in Figure 10. It is obvious that the speed value in channel permeability and single crack is higher than the surrounding matrix, and the fluid flow is expected to be attracted and directed towards the higher permeability through the interface. These observations agree perfectly with the phase evolution plotted in Figure 9. The reasonable numerical results show the robustness and compatibility of the numerical algorithms proposed in this paper, as well as the importance of the interface between different subdomains.

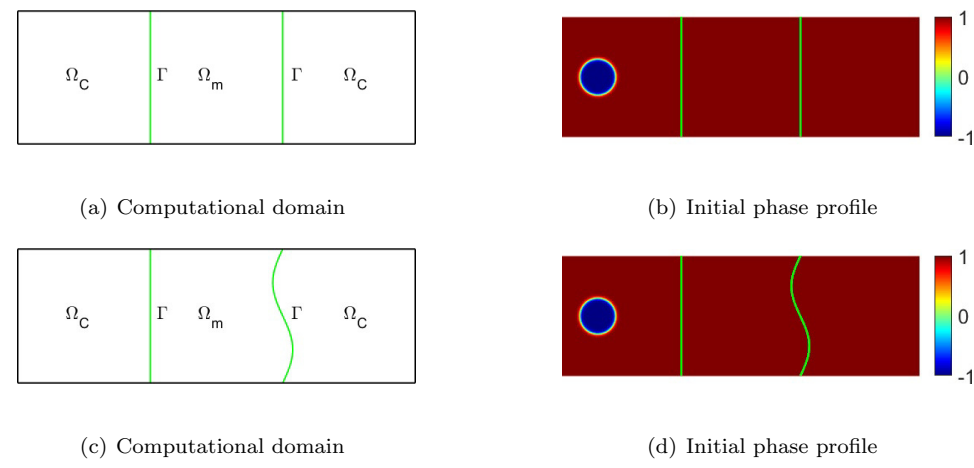


Fig. 7: Computational domains (left) and contour plots of initial phase functions (right).

Example 6: Buoyancy-driven flow.

In this test, we consider binary fluids with different densities to illustrate the effectiveness of proposed gPAV numerical method. We exploit Boussinesq approximation [16, 49] to deal with small ratio of density between two fluids, and simulate the dynamics of bubble in a heavier medium. The buoyancy-driven term $B := -g\phi(\rho_1 - \rho_2)$ to the right side of Darcy equation (2.1) and momentum equation (2.5) with respect

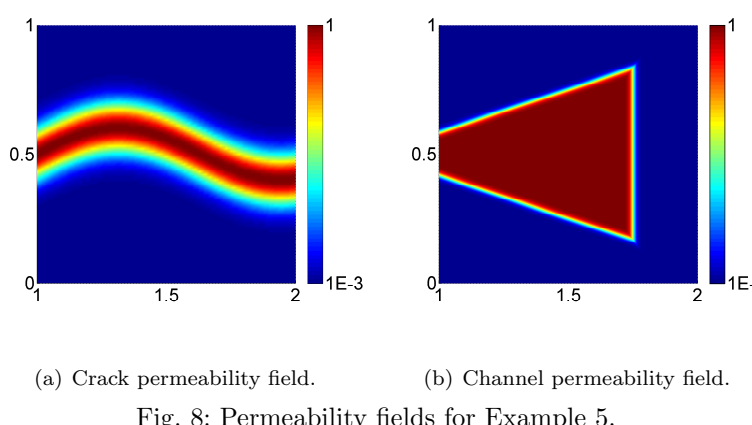


Fig. 8: Permeability fields for Example 5.

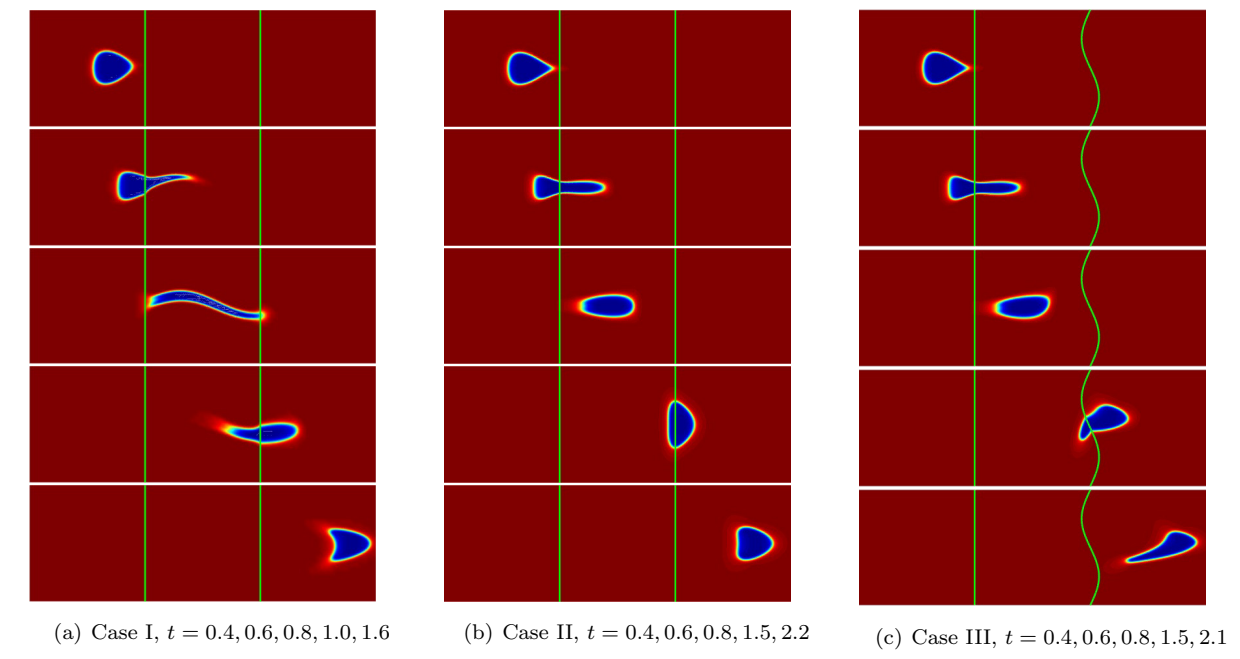


Fig. 9: The evolution of droplet in heterogeneous permeability medium for three cases from column by column.

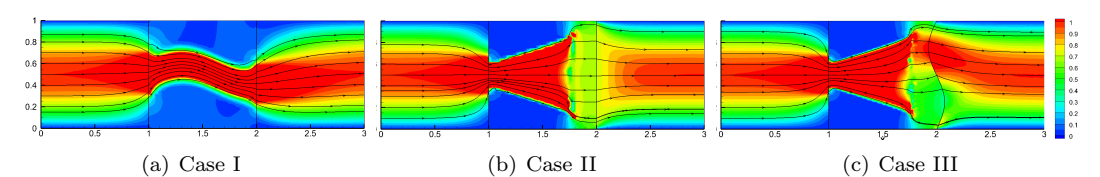


Fig. 10: Velocity and streamlines at t = 1.0 for three cases in Example 5.

to different densities ρ_1 and ρ_2 of binary fluids, \mathbf{g} is the gravitational acceleration with $\mathbf{g} = [0, g]^T$. Choosing parameters $\gamma=0.01,\,\epsilon=0.01,\,\nu=1,\,\mathbb{K}=0.1\mathbb{I},\,\rho_1=1,\,\rho_2=5,\,g=9.8$ and M=0.01 on domain $\Omega = [0,1] \times [0,2]$ associated with the porous media region $\Omega_m = [0,1] \times [1,2]$ and free flow region $\Omega_c = [0,1] \times [0,1].$

Firstly, we simulate a single rising bubble according to the following initial conditions for phase variable

$$\phi_0(x,y) = \tanh\left((0.2 - \sqrt{(x - 0.5)^2 + (y - 0.3)^2})/(\sqrt{2}\epsilon)\right). \tag{5.5}$$

Figure 11 shows the phase patters of a rising bubble from free fluid region to porous medium across the interface $\Gamma = [0,1] \times \{1\}$. The apparent deformation of the bubbles as they pass through the interface under the buoyancy force is observed, which is similar to the numerical results recorded in [10].

We further consider the evolutions of two coaxial bubbles [5, 61, 7] to verify the aptness of proposed gPAV numerical method. The initial position of two bubbles is given by

$$\phi_c^0(x,y) = 1 + \sum_{i=1}^2 \tanh\left((0.15 - \sqrt{(x-x_i)^2 + (y-y_i)^2})/(\sqrt{2}\epsilon)\right),\tag{5.6}$$

where $(x_1, y_1) = (0.5, 0.22)$ and $(x_2, y_2) = (0.5, 0.57)$. The other parameters are the same as in the case of a single rising bubble. The typical morphotypes of two rising bubbles are displayed in Figure 12. As expected, two bubbles rise dependently, coalesce to a single bubble, and eventually deform into a stable pattern. Similar numerical processes are presented in [24]. The reasonable results illustrate the validity of the numerical schemes.

The dynamics of bubbles are presented in Figure 12. One can clearly observe the coalescence of two kissing bubbles and shape deformation, eventually rising of a single droplet across the interface between two domains as recorded in Figure 11. From Figure 12, due to the difference in density between two fluids, we can see that the deformation of two droplets, then merge a single droplet, gradually evolve into the stable appearance as time evolved. The reasonable results illustrate the validity of the numerical schemes.

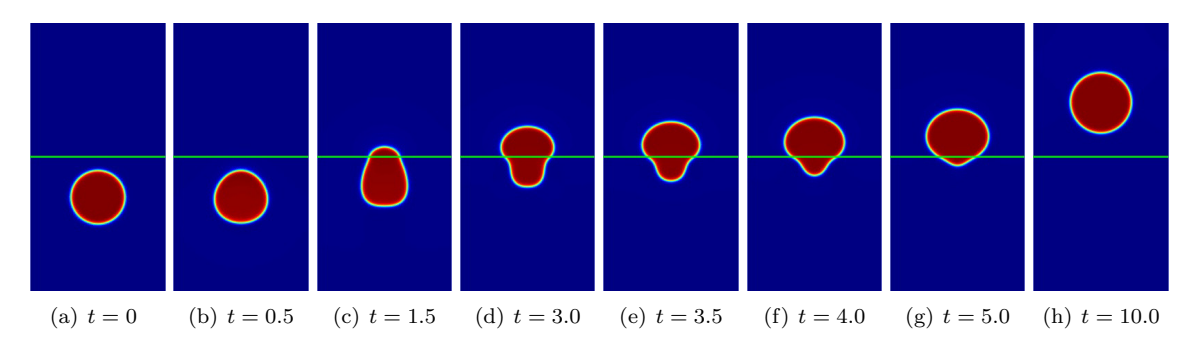


Fig. 11: The evolution of a rising bubble in a heavier medium from left to right row by row.

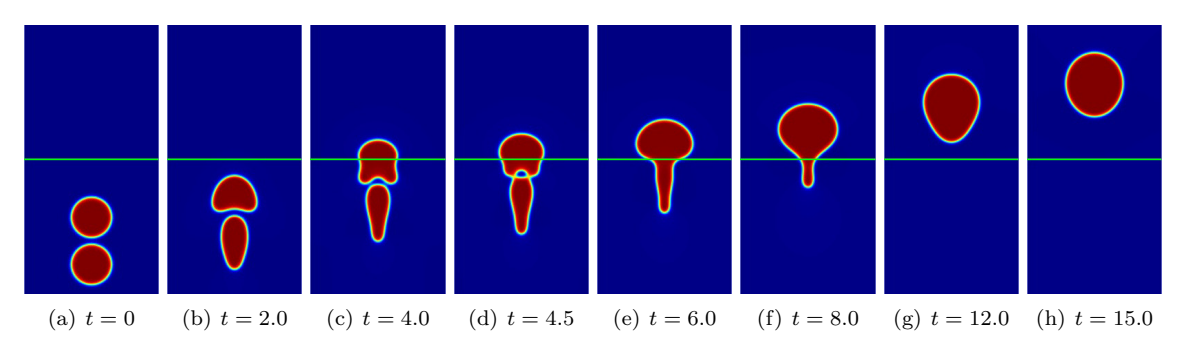


Fig. 12: The evolution of vertical rising bubbles in a heavier medium from left to right row by row.

6 Conclusions

In this paper, fully decoupled gPAV-CNLF and gPAV-BDF2 time-marching schemes are developed for numerically solving the CHNSD system in coupled free flow and porous media regions. Following the gPAV framework, we exploited the artificial compressible method to break the coupling of velocity and pressure in the Navier-Stokes equations. The unconditional stability in terms of a modified discrete energy is established for both the gPAV-CNLF and the gPAV-BDF2 algorithms. We only need to individually solve a sequence of linear algebraic system at each time level after splitting the unknown variables. The accuracy and energy stability of proposed gPAV methods are validated by numerical experiments. The boundary driven flow in filtering problem, the phenomenon of viscous fingering, buoyancy-driven flow with different densities are simulated to further verify the robustness of the numerical methods.

Declaration

Funding

The first author is partially supported by the NSFC, PR China grant 12371406, Natural Science Foundation of Guangdong Province, PR China 2023A1515010697. The work of the second author was partially supported by the National Science Foundation grants DMS-2310340.

Conflict of interests

The author Yali Gao declares that she has no conflict of interests during this study. The author Daozhi Han affirms that he has no conflict of interests in this study.

Data availability statement

All data generated or analysed during this study are included in this article.

References

- M.G. Armentano and M.L. Stockdale. Approximations by mini mixed finite element for the Stokes-Darcy coupled problem on curved domains. Int. J. Numer. Anal. Model., 18:203–234, 2021.
- 2. S. Bashir, J.M. Rees, and W.B. Zimmerman. Simulations of microfluidic droplet formation using the two-phase level set method. *Chem. Eng. Sci.*, 66(20):4733–4741, 2011.
- 3. A. Baskaran, J. S. Lowengrub, C. Wang, and S. M. Wise. Convergence analysis of a second order convex splitting scheme for the modified phase field crystal equation. *SIAM J. Numer. Anal.*, 51(5):2851–2873, 2013.
- 4. G. Beavers and D. Joseph. Boundary conditions at a naturally permeable wall. *J. Fluid Mech.*, 30:197–207, 1967.
- 5. G. Brereton and D. Korotney. Coaxial and oblique coalescence of two rising bubbles. In G. Tryggvason I. Sahin, editor, *Dynamics of Bubbles and Vortices Near a Free Surface*, volume 119. ASME, 1991.
- 6. M. Cai, M. Mu, and J. Xu. Numerical solution to a mixed Navier-Stokes/Darcy model by the two-grid approach. SIAM J. Numer. Anal., 47(5):3325–3338, 2009.
- 7. I. Chakraborty, G. Biswas, and P.S. Ghoshdastidar. A coupled level-set and volume-of-fluid method for the buoyant rise of gas bubbles in liquids. *Int. J. Heat Mass Tran.*, 58(1):240–259, 2013.
- 8. C.-Y. Chen, Y.-S. Huang, and J.A. Miranda. Diffuse-interface approach to rotating Hele-Shaw flows. *Phys. Rev. E*, 84:046302, 2011.
- 9. J. Chen, S. Sun, and X. Wang. A numerical method for a model of two-phase flow in a coupled free flow and porous media system. *J. Comput. Phys.*, 268:1–16, 2014.
- 10. W. Chen, D. Han, and X. Wang. Uniquely solvable and energy stable decoupled numerical schemes for the Cahn-Hilliard-Stokes-Darcy system for two-phase flows in karstic geometry. *Numer. Math.*, 137(1):229–255, 2017.
- 11. W. Chen, D. Han, X. Wang, and Y. Zhang. Uniquely solvable and energy stable decoupled numerical schemes for the Cahn-Hilliard-Navier-Stokes-Darcy-Boussinesq system. *J. Sci. Comput.*, 85(45):1–28, 2020.
- 12. W. Chen, S. Wang, Y. Zhang, D. Han, C. Wang, and X. Wang. Error estimate of a decoupled numerical scheme for the Cahn-Hilliard-Stokes-Darcy system. *IMA Numer. Analysis*, 42(3):2621–2655, 2022.
- 13. P. Chidyagwai and B. Riviére. Numerical modelling of coupled surface and subsurface flow systems. *Adv. Water Resour.*, 33:92–105, 2010.
- 14. Y.J. Choi and P.D. Anderson. Cahn-Hilliard modeling of particles suspended in two-phase flows. *Int. J. Numer. Meth. Fluids*, 69(5):995–1015, 2012.
- 15. P. G. Ciarlet. The finite element method for elliptic problems, volume 4 of Studies in Mathematics and its Applications. North-Holland Publishing Co., Amsterdam-New York-Oxford, 1978.
- 16. C. Collins, J. Shen, and R. Jari. An efficient, energy stable scheme for the Cahn-Hilliard-Brinkman system. *Commu. Comput. Phys.*, 13:929–957, 2013.

17. L. Cueto-Felgueroso and R. Juanes. A phase-field model of two-phase Hele-Shaw flow. *J. Fluid Mech.*, 758:522–552, 2014.

- 18. V. DeCaria, T. Illiescu, W. Layton, M. McLaughlin, and M. Schneier. An artificial compression reduced order model. SIAM J. Numer. Anal., 58:565–589, 2020.
- 19. L. Dedè, H. Garcke, and K.F. Lam. A Hele-Shaw-Cahn-Hilliard model for incompressible two-phase flows with different densities. *J. Math. Fluid Mech.*, 20(2):531–567, 2018.
- 20. A. Diegel, X. Feng, and S. Wise. Analysis of a mixed finite element method for a Cahn-Hilliard-Darcy-Stokes system. SIAM J. Numer. Anal., 53(1):127–152, 2015.
- 21. X.L. Feng, T. Tang, and J. Yang. Stabilized Crank-Nicolson/Adams-Bashforth schemes for phase field models. *East Asian J. Appl. Math.*, 3:59–80, 2013.
- 22. R. B. Ferreira, D.S. Falcão, V.B. Oliveira, and A.M.F.R. Pinto. Numerical simulations of two-phase flow in proton exchange membrane fuel cells using the volume of fluid method-A review. *J. Power Sour.*, 277:329–342, 2015.
- 23. Y. Gao, D. Han, X.-M. He, and U. Rüde. Unconditionally stable numerical methods for Cahn-Hilliard-Navier-Stokes-Darcy system with different densities and viscosities. *J. Comput. Phys.*, 454:110968, 2022.
- 24. Y. Gao, X. He, T. Lin, and Y. Lin. Fully decoupled energy-stable numerical schemes for two-phase coupled porous media and free flow with different densities and viscosities. *ESAIM Math. Model. Numer. Anal.*, 57(3):1323–1354, 2023.
- 25. Y. Gao, X. He, L. Mei, and X. Yang. Decoupled, linear, and energy stable finite element method for the Cahn-Hilliard-Navier-Stokes-Darcy phase field model. *SIAM J. Sci. Comput.*, 40(1):B110–B137, 2018.
- Y. Gao, R. Li, X. He, and Y. Lin. A fully decoupled numerical method for Cahn-Hilliard-Navier-Stokes-Darcy equations based on auxiliary variable approaches. J. Comput. Appl. Math., 436:115363, 2024
- 27. V. Girault and B. Rivière. DG approximation of coupled Navier-Stokes and Darcy equations by Beaver-Joseph-Saffman interface condition. SIAM J. Numer. Anal, 47(3):2052–2089, 2009.
- 28. Z. Guan, C. Wang, and S.W. Wise. A convergent convex splitting scheme for the periodic nonlocal Cahn-Hilliard equation. *Numer. Math.*, 128:277–406, 2014.
- 29. J.-L. Guermond and P. Minev. High-order time stepping for the Navier-Stokes equations with minimal computational complexity. *J. Comput. Appl. Math.*, 310:92–103, 2017.
- 30. J.-L. Guermond, P. Minev, and J. Shen. An overview of projection methods for incompressible flows. *Comput. Methods Appl. Mech. Engrg.*, 195(44):6011–6045, 2006.
- 31. R. Guo, Y. Xia, and Y. Xu. An efficient fully-discrete local discontinuous Galerkin method for the Cahn-Hilliard-Hele-Shaw system. *J. Comput. Phys.*, 264:23–40, 2014.
- 32. D. Han, D. Sun, and X. Wang. Two-phase flows in karstic geometry. *Math. Methods Appl. Sci.*, 37(18):3048–3063, 2014.
- 33. D. Han and X. Wang. A second order in time, decoupled, unconditionally stable numerical scheme for the Cahn-Hilliard-Darcy system. *J. Sci. Comput.*, 77(2):1210–1233, 2018.
- 34. D. Han, X. Wang, Q. Wang, and Y. Wu. Existence and weak-strong uniqueness of solutions to the Cahn-Hilliard-Navier-Stokes-Darcy system in superposed free flow and porous media. *Nonlinear Anal.*, 211:112411, 2021.
- 35. D. Han, X. Wang, and H. Wu. Existence and uniqueness of global weak solutions to a Cahn-Hilliard-Stokes-Darcy system for two phase incompressible flows in karstic geometry. *J. Differential Equations*, 257(10):3887–3933, 2014.
- 36. N.S. Hanspal, A.N. Waghode, V. Nassehi, and R.J. Wakeman. Numerical analysis of coupled Stokes/Darcy flow in industrial filtrations. *Transp. Porous Media*, 64:73–101, 2006.
- 37. X.-M. He, N. Jiang, and C. Qiu. An artificial compressibility ensemble algorithm for a stochastic Stokes-Darcy model with random hydraulic conductivity and interface conditions. *Int. J. Numer. Methods Eng.*, pages 1–28, 2019.
- 38. N. Jiang, Y. Li, and H. Yang. An artificial compressibility Crank-Nicolson Leap-Frog method for the Stokes-Darcy model and application in ensemble simulations. *SIAM J. Numer. Anal.*, 59(1):401–428, 2021.
- 39. N. Jiang and H. Yang. Stabilized scalar auxiliary variable ensemble algorithms for parameterized flow problems. SIAM J. Sci. Comput., 43:A2869–A2896, 2021.

40. M. Karam and T. Saad. High-order pressure estimates for projection-based Navier-Stokes solvers. J. Comput. Phys., 452:110925, 2022.

- 41. J. Kou, X. Wang, S. Du, and S. Sun. An energy stable linear numerical method for thermodynamically consistent modeling of two-phase incompressible flow in porous media. *J. Comput. Phys.*, 451:110854, 2022.
- 42. A. Labovsky, W.J. Layton, C.C. Manica, M. Neda, and L.G. Rebholz. The stabilized extrapolated trapezoidal finite-element method for the Navier-Stokes equations. *J. Comput. Phys.*, 198(9-12):958–974, 2009.
- 43. W. Layton, H. Tran, and C. Trenchea. Analysis of long time stability and errors of two partitioned methods for uncoupling evolutionary groundwater-surface water flows. SIAM J. Numer. Anal., 51(1):248–272, 2013.
- 44. H. G. Lee, J. Lowengrub, and J. Goodman. Modeling pinchoff and reconnection in a Hele-Shaw cell. I. The models and their calibration. *Phys. Fluids*, 14(2):492–513, 2002.
- 45. L. Lin, X. Liu, and S. Dong. A gPAV-based unconditionally energy-stable scheme for incompressible flows with outflow/open boundaries. *Comput. Methods Appl. Mech. Engrg.*, 365:112969, 2020.
- 46. L. Lin, N. Ni, Z. Yang, and S. Dong. An energy-stable scheme for incompressible Navier-Stokes equations with periodically updated coefficient matrix. *J. Comput. Phys.*, 418:109624, 2020.
- 47. S. Litster, D. Sinton, and N. Djilali. Ex situ visualization of liquid water transport in PEM fuel cell gas diffusion layers. *J. Power Source*, 154(1):95–105, 2006.
- 48. C. Liu, D. Ray, C. Thiele, L. Lin, and B. Riviere. A pressure-correction and bound-preserving discretization of the phase-field method for variable density two-phase flows. *J. Comput. Phys.*, 449:110769, 2022.
- 49. C. Liu and J. Shen. A phase field model for the mixture of two incompressible fluids and its approximation by a Fourier-spectral method. *Phys. D*, 179(3-4):211–228, 2003.
- 50. J. Lowengrub and L. Truskinovsky. Quasi-incompressible Cahn-Hilliard fluids and topological transitions. R. Soc. Lond. Proc. Ser. A Math. Phys. Eng. Sci., 454(1978):2617–2654, 1998.
- 51. Q. Pan, C. Chen, Y.J. Zhang, and X. Yang. A novel hybrid IGA-EIEQ numerical method for the Allen-Cahn/Cahn-Hilliard equations on complex curved surfaces. *Comput. Methods Appl. Mech. Engrg.*, 404:115767, 2023.
- 52. Y. Qian, Z. Wang, F. Wang, and S. Dong. gPAV-based unconditionally energy-stable schemes for the Cahn-Hilliard equation: Stability and error analysis. *Comput. Methods Appl. Mech. Engrg.*, 372:113444, 2020.
- 53. Z. Qiao, S. Sun, T. Zhang, and Y. Zhang. A new multi-component diffuse interface model with Peng-Robinson equation of state and its scalar auxiliary variable (SAV) approach. *Commun. Comput. Phys.*, 26(5):1597–1616, 2019.
- 54. P.G. Saffmann and G.I. Taylor. The penetration of a fluid into a porous medium or Hele-Shaw cell containing a more viscous liquid. *Proc. R. Soc. Lond. Ser. A*, 245(1242):312–329, 1958.
- 55. J. Shen, C. Wang, X. Wang, and S.M. Wise. Second-order convex splitting schemes for gradient flows with Ehrlich-Schwoebel type energy: application to thin film epitaxy. SIAM J. Numer. Anal., 50(1):105–125, 2012.
- 56. J. Shen, J. Xu, and J. Yang. A new class of efficient and robust energy stable schemes for gradient flows. SIAM Rev., 61(3):474–506, 2019.
- 57. J. Shen and X. Yang. Numerical approximations of Allen-Cahn and Cahn-Hilliard equations. *Discrete Contin. Dyn. Syst.*, 28:1169–1691, 2010.
- 58. J. Shen and X. Yang. Decoupled, energy stable schemes for phase-field models of two-phase incompressible flows. SIAM J. Numer. Anal., 53(1):279–296, 2015.
- 59. P. Song, C. Wang, and I. Yotov. Domain decomposition for Stokes-Darcy flows with curved interfaces. *Proc. Comput. Sci.*, 18:1077–1086, 2013.
- 60. P.T. Sun, G. Xue, C.Y. Wang, and J.C. Xu. A domain decomposition method for two phase transport model in the cathode of a polymer electrolyte fuel cell. *J. Comput. Phys.*, 228:6016–6036, 2009.
- 61. M. van Sint Annaland, N.G. Deen, and J.A.M. Kuipers. Numerical simulation of gas bubbles behaviour using a three-dimensional volume of fluid method. *Chem. Eng. Sci.*, 60(11):2999–3011, 2005.
- 62. C. Xu, C. Chen, X. Yang, and X.-M. He. Numerical approximations for the hydrodynamics coupled binary surfactant phase field model: second order, linear, unconditionally energy stable schemes. *Commun. Math. Sci.*, 17(3):835–858, 2019.

63. Y. Yan, W. Chen, C. Wang, and S.M. Wise. A second-order energy stable BDF numerical scheme for the Cahn-Hilliard equation. *Commun. Comput. Phys.*, 23(2):572–602, 2018.

- 64. J. Yang and J. Kim. Energy dissipation-preserving time-dependent auxiliary variable method for the phase-field crystal and the Swift-Hohenberg models. *Numer. Algorithms*, 89(4):1865–1894, 2022.
- 65. X. Yang. On a novel fully decoupled, second-order accurate energy stable numerical scheme for a binary fluid-surfactant phase-field model. SIAM J. Sci. Comput., 43(2):B479–B507, 2021.
- 66. X. Yang and D. Han. Linearly first- and second-order, unconditionally energy stable schemes for the phase field crystal equation. *J. Comput. Phys.*, 330:13–22, 2017.
- 67. X. Yang and X. He. A fully-discrete decoupled finite element method for the conserved Allen-Cahn type phase-field model of three-phase fluid flow system. *Comput. Meth. Appl. Mech. Eng.*, 389:114376, 2022.
- 68. Z. Yang and S. Dong. A roadmap for discretely energy-stable schemes for dissipative systems based on a generalized auxiliary variable with guaranteed positivity. *J. Comput. Phys.*, 404:109121, 2020.
- 69. G. Zhang, X.-M. He, and X. Yang. A fully decoupled linearized finite element method with second-order temporal accuracy and unconditional energy stability for incompressible MHD equations. *J. Comput. Phys.*, 448:#110752, 2022.
- 70. H. Zhang, X. Yang, and J. Zhang. Stabilized invariant energy quadratization (S-IEQ) method for the molecular beam epitaxial model without slope section. *Int. J. Numer. Anal. Model.*, 18:642–655, 2021
- 71. G. Zhu, J. Kou, J. Yao, A. Li, and A. Sun. A phase-field moving contact line model with soluble surfactants. *J. Comput. Phys.*, 405:109170, 2020.
- 72. P. Zhu and L. Wang. Passive and active droplet generation with microfluidics: a review. *Lab Chip*, 17(1):34–75, 2017.